Condensation Control in Glazed Flat Plate Solar Water Heaters

Joji Oshikiri

A thesis submitted in partial fulfillment of the requirements for the degree of Master of Engineering, Auckland University of Technology, 2012.

Abstract

Flat plate solar thermal collectors are used around the world in both domestic and industrial fields as a simple and effective method to heat water. Avoiding condensation in solar collectors at night is a crucial issue in terms of their durability and performance.

During the night the temperature of the collector will often drop below the ambient temperature due to thermal radiation in the cold air. In climates where the air at night becomes saturated with humidity, condensation will form both on the inside and outside of the collector glazing. Condensation on the glazing means energy is wasted in evaporating the moisture throughout the following day. If too much condensation occurs on the inside of the glazing, it will drip on to the absorber surface, which will consequently lead to long-term damage.

The objective of this study was to undertake the development of a model, and to validate it. This will determine the frequency of condensation in glazed flat plate solar water heaters and the all parameters which are involved in this phenomenon.

The numerical model showed that climatic factors including relative humidity, ambient temperature and wind speed determine the frequency of condensation for any given location. However, it also reveals that the frequency of condensation can be modified by altering the ventilation inside the collector, the slope of the collector and most significantly by using low emissivity coating on the glazing layer.

Acknowledgements

There are so many people who deserve special thanks for contributing to this thesis.

First of all, I wish to express my deepest thanks to my supervisor Dr Tim Anderson for guiding me into the right direction for this project and helped and cared about my progress in the project. I feel motivated and encouraged every time when I face the problems of the research. Without his encouragement and guidance this research would not have accomplished.

I would like to show my greatest appreciation to Prof. Ahmed-Al Jumaily. I can't say thank you enough for his tremendous support and help through the duration of my studies.

I appreciate the help from the electrician members from AUT engineering department. Thank you all for sharing the academic knowledge with me, showing me lots of useful skills, and bright ideas for experiments.

Special thanks to the National Institute of Water and Atmospheric Research (NIWA). They provided a great deal of weather information data in New Zealand, and it was necessary to accomplish my research.

My family, the most important support team in my life, have been given me endless support and care through the duration of my studies.

I am indebted to ‘Ference Kish’ and ‘Mari Oshikiri’ who helped to create the numerical model, and there are so many friends that I must say thank you, they are great people to work and talk with.

Table of Contents

List of Figures

List of Tables

NOMENCLATURE

A_c	Cover area
A_p	Absorber area
a_c	The solar absorptance of the cover
C_c	The thermal capacity of the cover (J/kgK)
C_p	The thermal capacity of the absorber (J/kgK)
C_{pa}	Specific heat of air (J/kg℃)
C_s	Stefan-Boltzman constant (W/m^2K^4)
DT_{sky}	Sky temperature depression
e_g	The thickness of the air gap (m)
e_i	The thickness of the insulation (m)
F_{12}	View factor
g	Gravitational constant (m/s^2)
G	The solar irradiation on the solar collector
Gr	Grashof number
h	The height of the airgap
h_{cb}	Conduction through the rear insulation
h_{cg}	Natural convection in the air gap
h_{fg}	The latent heat of water (J/kg)
h_{rg}	Thermal radiation in the air gap

h_{co}	Convection from the outside of the cover
h_{ro}	Thermal radiation from the outside of the cover
h_{vg}	Ventilation of the air gap
h_w	Convective coefficient
K_a	Von Karman's constant
k_g	Thermal conductivity of air (M/m℃)
k_i	The coefficient of thermal conduction of the rear insulation
k_0	Thermal conductivity of the ambient air (W/m℃)
L	Characteristic length (m)
m_{da}	The mass of dry air
m_w	The mass of the water vapor
m_{vg}	Total mass flow of aqueous vapor and dry air (kg/sm^2)
Nu_g	Nusselt number for the gap
Nu_o	Nusselt number for the convection
Nu_{lam}	Nusselt number for laminar flow
Nu_{turb}	Nusselt number for turbulent flow
P_a	Atmospheric pressure in open air (Pa)
P_c	Pressure inside the collector
P_{ca}	Parcial pressure of dry air inside the collector
P_{cw}	Parcial pressure of waster vapor inside the collector
P_r	Prandtl number for the air
P_w	Partial pressure of aqueous vapour

P_{wa}	Partial pressure of water in the open air
P_{wg}	Partial pressure of water in the air of the air gap
$P_{ws}(T_c)$	Water vapor saturation pressure of the cover temperature (Pa)
$P_{ws}(T_{dewa})$	Water vapor saturation pressure of the dew point temperature (pa)
q_{ei}	Evaporation heat loss from the inside of the cover
q_{eo}	Evaporation heat loss from the outside of the cover
Ra	The gas constant for the gap
Ra_g	Raleigh number for the gap
Re	Reynolds number for forced convection
Re′	Reynolds number for natural convection
Re_+	Reynolds number for forced and natural convection
RH	Relative Humidity
s	Slope of the collector (degree)
T_a	The ambient temperature
T_c	The temperature of the cover
T_{dewa}	The dew point temperature
T_i	The temperature inside the collector
T_p	The temperature of the absorber
T_s	The temperature of the “black body”
t	Time
V	The specific volume of the moist air
V_g	The mass of the air gap
V_w	Wind velocity at the collector cover (m/s)

V_Z	Wind velocity in level Z
v_1	The wind speed at height h_1
v_2	The wind speed at height h_2
W	Absolute humidity
W_a	Absolute humidity ambient
W_g	Absolute humidity of air in the air gap
z	Vertical co-ordinate
z_0	The roughness length
α	The angular absorptance of the absorber plate
β	Volumetric coefficient of expansion of air
γ	The value of shear
ΔP	The difference pressure
ε_p	Emissivity of the absorber plate
ε_c	Emissivity of the cover
ε_{sky}	Emissivity of the sky
υ	Kinematic viscosity of ambient air (m^2/s^2)
ρ	The density of the air
$\rho(T_a, p_{wa})$	The density of the open air
ρ_a	The density of dry air
$\rho_a(\frac{T_p + T_c}{2}, p_{wg})$	The density of the air in the air gap
ρ_d	Reflectance
τ	The transmittance of the cover system at the desired angle
$\tau\alpha$	The transmission absorption product of the solar collector

Chapter 1: Introduction

Modern society relies deeply on the use of fossil fuels, and it is generally understood that they cause some negative impacts on the environment. Solar energy is a promising solution to this, as it can substitute fossil fuels in a clean and renewable manner. The use of solar water heating is widespread in Greece, Turkey, Israel, Australia, Japan, Austria and China. Solar water heating is cost effective and lasts for over 20 years even though several elements might need replacing sooner (Government of Bermuda, 2012). However, its performance decreases due to the degradation of the materials inside the collector. A great number of studies suggest that the main reason for its corrosion could be condensation inside of the collector (Kohl et al, 2003)

The basic mechanism of solar water heating systems is to create energy to heat water through solar panels which are attached to the roof. Although there are two types of solar water heating panels which are flat plate and evacuated tube collectors, flat plat collectors are more widespread. Flat plate connectors are made up of the absorber, a low-iron solar safety glass cover, header and flow tubes, a frame and insulation as shown in Figure 1. The flat plate collectors absorb the sun light and convert heat to warm water, which is accumulated in a hot water cylinder. The absorber is placed in the center of the solar collector tube, it is usually made from a collection of multiple strips of metal, or either copper aluminum. The absorber is normally black since it can absorb more heat (Figure 2).

Normally, a boiler or immersion heater can be used as a back up to heat water further to reach the temperature set by the cylinders thermostat when the solar water heating system is not already at that temperature. (The cylinder thermostat should be set at 60 degrees centigrade.)

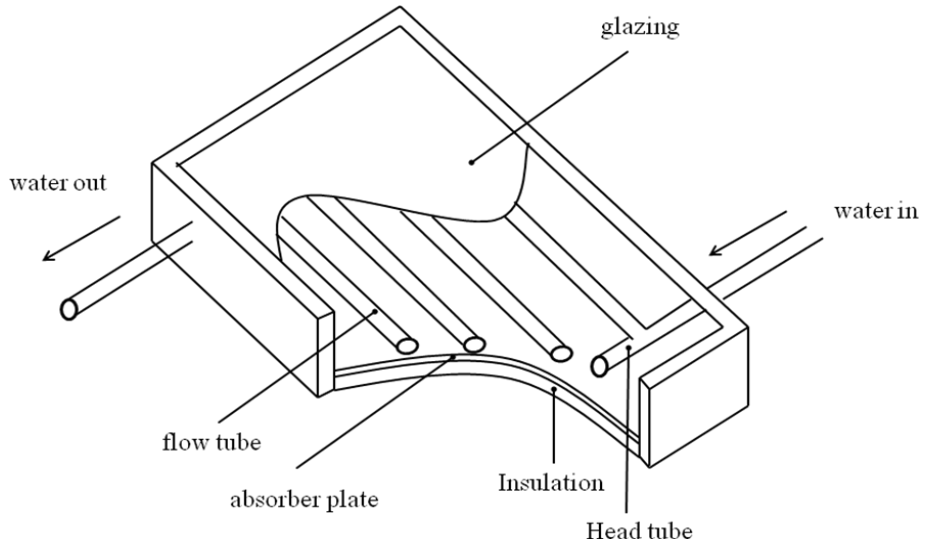

Figure 1: Elements of a flat plate solar water heating system

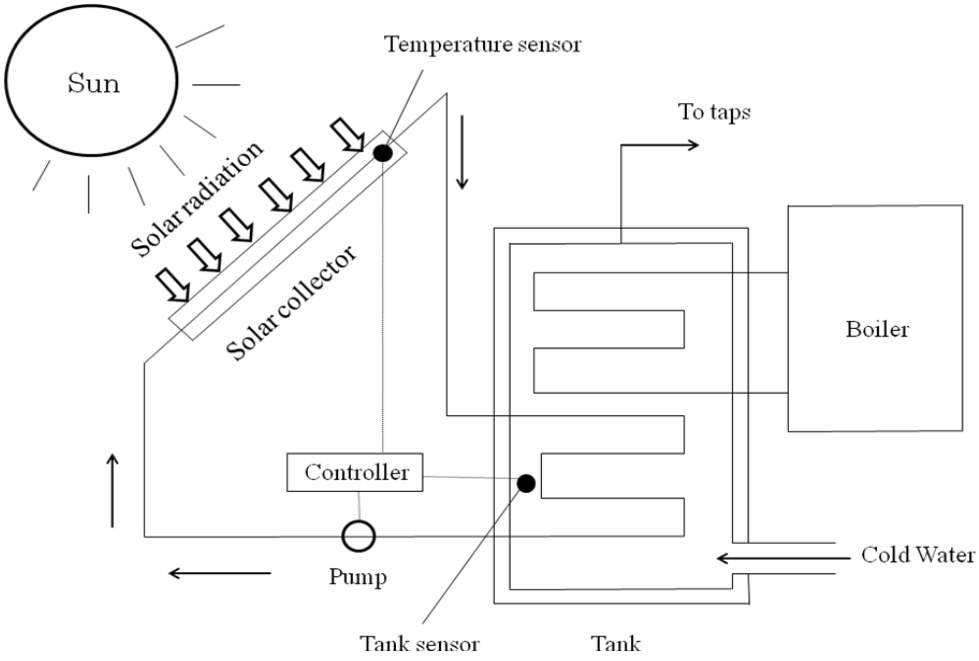

Figure 2: Over all view of the solar water heating system

Corrosion due to condensation and performance of solar water heating systems is a significant problem in New Zealand (Moller, 2012). Condensation is a natural phenomenon that normally occurs in buildings and vehicles due to changes in temperature and humidity. Solar thermal flat plate collectors also suffer from condensation problems, particularly, in cold areas with high relative humidity. A great deal of moisture condensation can occur even in a small solar thermal flat plate. Repeated condensation can lead to a degrading of the collector over time.

The mechanism of condensation in a solar thermal flat plate is driven by the release of heat into the atmosphere by radiation particularly at night. The temperature in the collector falls below the dew point temperature and condensation forms on inside the glazing of the collector. Figure 3 shows condensed water on the glazing of solar collectors. The existence of water can cause damage to the collector surface and create unfavorable microclimatic conditions for the internal materials. In addition to this, energy must be used to evaporate the moisture the next day.

This project aims to develop the understanding of the role that condensation plays on collector performance, as well as addressing ways of minimizing the impact it has on solar collectors. This study highlights condensation problems on the outer surface of the collector, and it was assumed that condensation occurs when the cover temperature drops below than the dew point temperature of the ambient air.

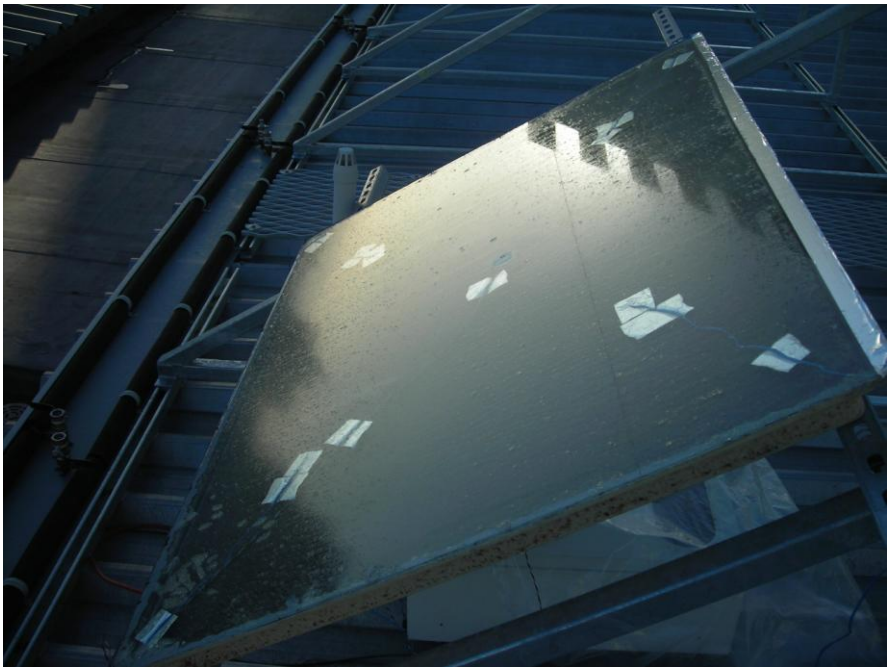

Figure 3: Condensation on the outer surface of the collector glazing

Chapter 2: Literature review

This section will highlight previous research, that is related to the condensation problems of solar collectors. The following section will discuss some of the causes and cures of condensation: ventilation rate, heat loss from outer cover, insulation materials, sky temperature and simulation of the microclimate.

2-1 The causes and cures of the condensation problems

Condensation will take place on any surface that has a temperature which is lower than the dew point temperature of the air that it is in contact with it. Condensation could happen either on the surface of the inner window or outer window. One example of this is when condensation occurs on a winter's morning on the surface of the inner window because warm humid air inside is cooled by the window which is cooled by the outside atmosphere. Condensation usually occurs on windows first because they normally have the lowest temperature of any of the interior surfaces in the house (Dickens, 1963). Secondly, condensation sometimes occurs on the surface of the outer window, for instance, in summer the condensation can occur in a room which is cooled by an air conditioner and when outside humidity is quite high the reason for this is that the outside moisture is cooled by windows.

The two most effective solutions to prevent condensation are having appropriate ventilation and using thermal insulation materials. Normally, it is important to gain enough space so that either wind or a fan can pass through to stop condensation. Secondly, applying thermal insulation materials is also effective since thermal insulation materials help to stop heat transfer between objects in thermal contact (Dickens, 1963). For solar hot water heating system, having appropriate ventilation and using thermal insulation materials also could be important factors to prevent condensation.

2-2 Ventilation rate

Solar collectors often show condensed water in the glazing, since they exchange air and moisture with the environment. The moisture increases the rate of corrosion in the collector. It has been known that the ventilation rate is key to keeping the collector dry; however, it allows increases thermal losses. The research group MSTC (Materials for Solar Thermal Collectors) of SHCP (the solar heating an cooling Programme) of IEA (International Energy Agency) developed a method for ventilation rate measurements and examined it by using a round robin test of the same collector in several laboratories: IBE (Denmark), TNO (Netherlands), SPF (Switzerland) and ISE (Germany). The method measured the air flow rate in the back-plane of the collectors while putting a positive and negative pressure difference in the order of 0.1-30 Pa between collector and environment. The results which are shown in Figure 4 and Figure 5 describe the function of pressure and flow rate of eight different ventilated commercial collectors. It was concluded that the ventilation rate can be described by the flow-rate in collector-volumes per hour at a pressure difference of 1 Pa (Kohl et al. 2007).

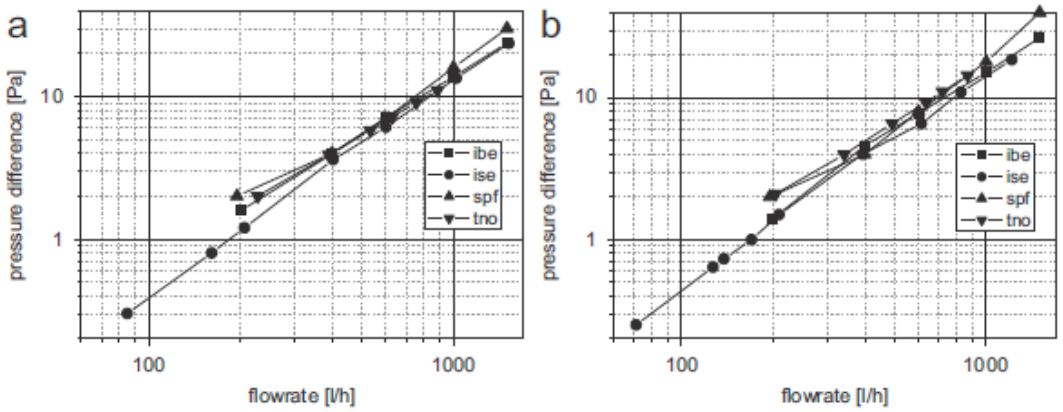

(a) (b)

Figure 4: Measurement of the ventilation rate of a reference collector in different laboratories (a) Under-pressure (b) Over-pressure
(Kohl et al, 2007,p. 723)

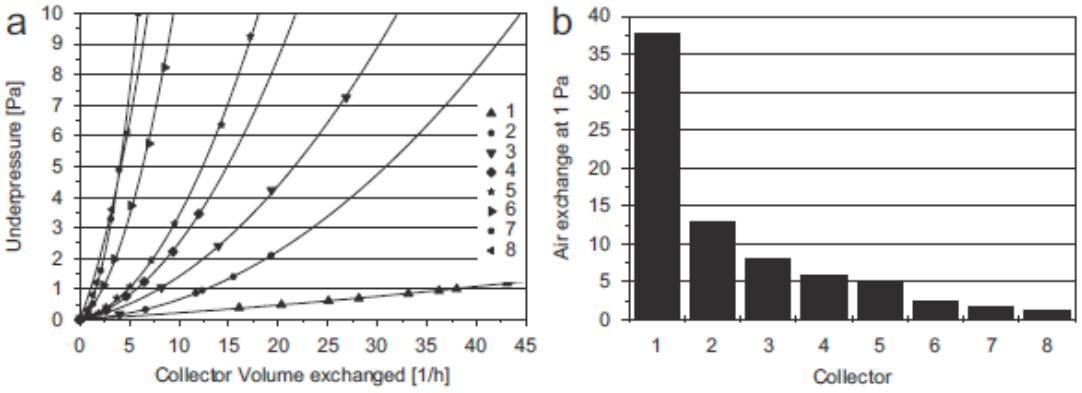

Figure 5: Measurement of the ventilation rate of different collectors (Kohl et al. 2007)
(a) Measurements and exponential fit. (b) Ventilation rate at 1 Pa
(Kohl et al, 2007,p. 723)

In the experiments, velocity of the air-flow through the ventilation hole of a flat plate collector during a day was measured (displayed in Figure 6). The flow-velocity was measured by a micro-anemometer which was placed in front of a ventilation hole of a controlled ventilated collector. In addition, the air temperature in collector air gap and ambient air were measured. Figure 6 indicates that the air exchange during the night time period reverses in direction and the volume is almost half of the daytime. When the temperature falls below the dew point, gathering of moisture within the collector takes place (Kohl et al. 2007).

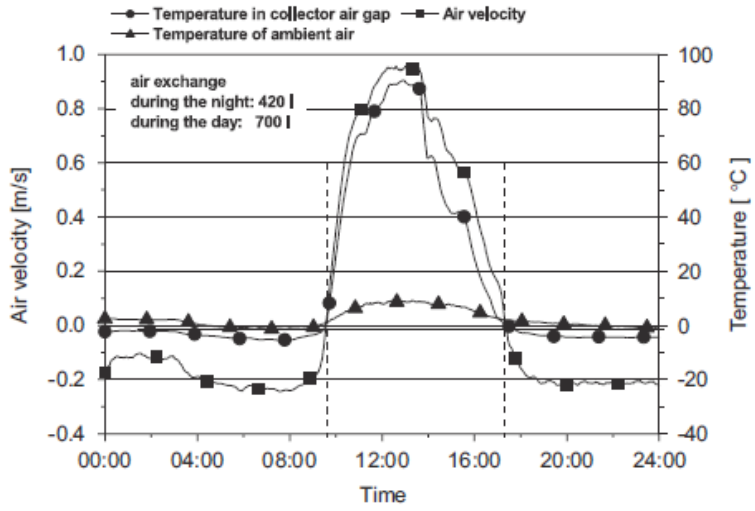

Figure 6: Velocity of the air-flow through the ventilation hole of a flat plate collector during a sunny winter day (Kohl et al, 2007,p. 722)

2-3 Heat loss from outer cover of solar collectors

The surface of a flat plate solar collector releases its heat due to the radiative and convective heat transfer processes. The wind induced convective heat transfer often dominates the magnitude of the surface heat loss. Consequently, the performance of a flat solar plate solar collector is significantly influenced by the convective heat transfer coefficient due to wind.

Duffie and Beckman (1991) stated the relationship of the convective coefficient to wind speed was give by equation (1)

$$h_w = 5.7 + 3.8V_w \quad (1)$$

Where V_w is the wind speed in m/s and h_w is the convective heat transfer coefficient $W/m^2{}^\circ\mathrm{C}$. However, Kumar et al (1997) published a different equation for wind heat transfer coefficients for different wind spends. The approximate linear correlation was given by equation (2).

$$h_w = 10.03 + 4.687V_w \quad (2)$$

2-4 Sky temperature

All objects exchange thermal radiation with surrounding objects and with the atmosphere, and at night the surface of a collector exchanges the radiation to the cold sky. To understaind the performance of solar collectors, it is important to know the actual sky temperature. However, it is difficult to measure the actual sky temperature.

In order to determine the heat exchange between the surface and the cold night sky, the clear sky emissivity value is important to understand. The sky emissivity is give by equation (3) (Parker, 2005).

$$\varepsilon_{sky} = 0.711 + 0.56(T_{dp}/100) + 0.73(T_{dp}/100)^2 \quad (3)$$

One of the parameters which determine the performance of a radiator is sky temperature depression which calculated as the difference between the ambient air temperature and the sky temperature (Argiriou et al. 1994).

$$DT_{sky} = (1 - \varepsilon_{sky}^{1/4})T_a \quad (4)$$

In addition, Kohl et al (2004) suggested equation (5) as a simple way to calculate the sky tempertuare. On the other hand, Duffie and Beckman (2006) published the equation (6) which was strengthened since equation (6) used not only the ambient temperature but also the hour from midnight (t) and the dew point temperature.

$$T_s = 0.0552 \cdot T_a^{1.5} \quad (5)$$

$$T_s = T\left[0.711 + 0.0056T_{dp} + 0.000073T_{dp}^2 + 0.13\cos(15t)\right]^{\frac{1}{4}} \quad (6)$$

2-5 Measurement and optimization of the micro-climate

To determine the humidity time constant in solar collectors, Kohl et al. (2007) created a climatic cabinet. The ambient climate condition in the cabinet was kept at 30℃ and 95% relative humidity at an inclinating angle of 45 degree. The collectors were also pre-conditioned at 25 degree Celsius with a humidity of 45%. The heat-transfer-fluid helped to keep the absorber temperature at 40℃. The collector was moved into the cabinet quickly and the relative humidity in the air-gap was measured. The results are shown in Figure 7.

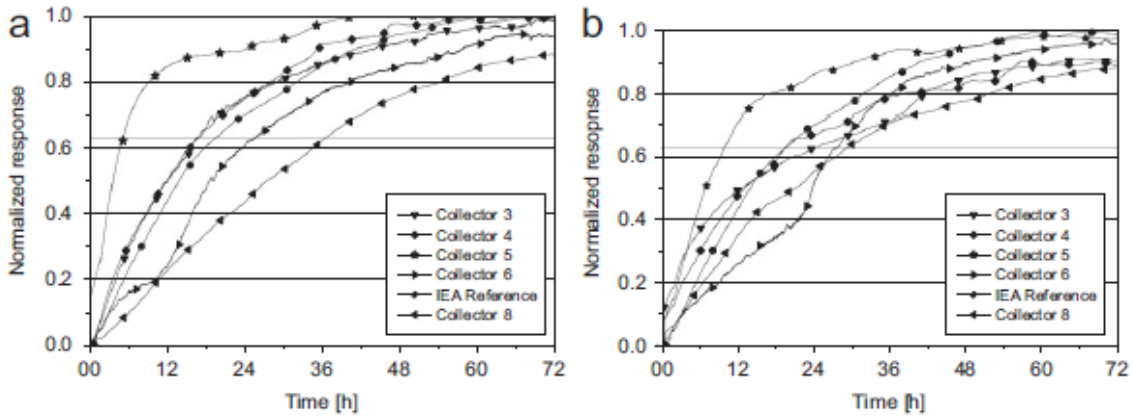

Figure 7: Response function of the humidity in commercial collectors after fast changes of the ambient humidity normalized to the maximum relative humidity (a) collectors as received, (b) collectors as in (a) but after optimizing the ventilation rate.

(Kohl et al, 2007,p. 724)

The same collectors were examined under simulated working conditions outdoors. As shown in Figure 8, the measurement of the air gap humidity is shown as frequency distribution functions.

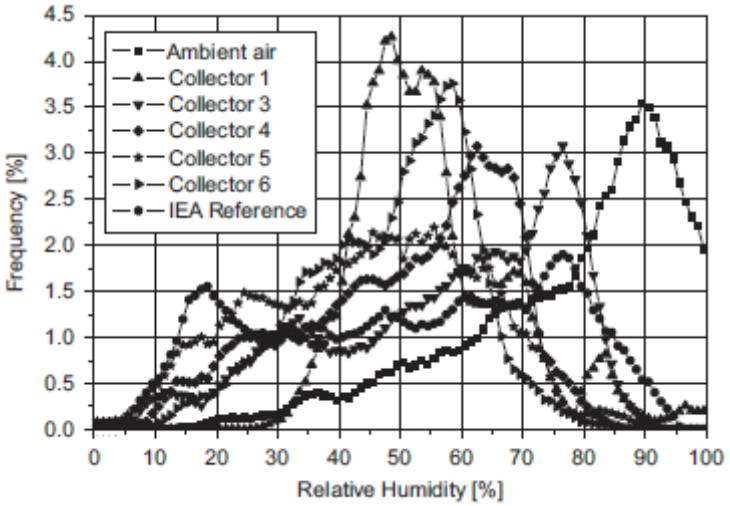

Figure 8: Frequency distribution of the humidity in the air-gap of different commercial collectors. (Kohl et al, 2007,p. 725)

As described in Figure 9 (a), variation of the ventilation rate only slightly changes in wetness behavior. However, a change of the insulation materials has a significant impact on changes in the wetness behavior (Figure 9 (b)). Consequently, both the ventilation and insulation materials inside the collector are important for optimization of the microclimate in collectors.

Kohl et al. 2007 also suggested that ventilation holes be placed on diagonally opposite corners because diagonal ventilation is more effective than dispersed ventilation holes along the edges. The effect was obviously reduced if insulation materials cover the ventilation holes (Figure 10) (Kohl et al. 2007).

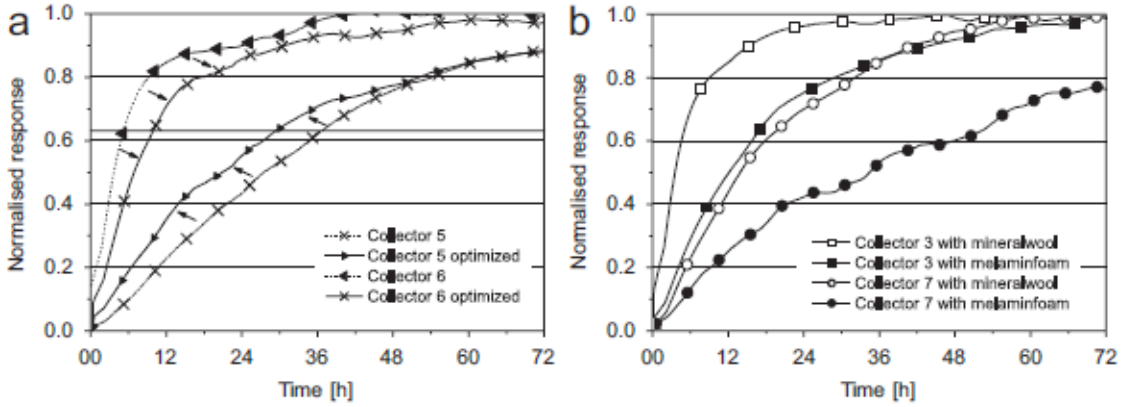

Figure 9: Impact of changes on the micro-climate on the humidity response function of collectors normalized to the maximum relative humidity (a) changing the ventilation rate, (b) changing the insulation material (Kohl et al, 2007,p. 725)

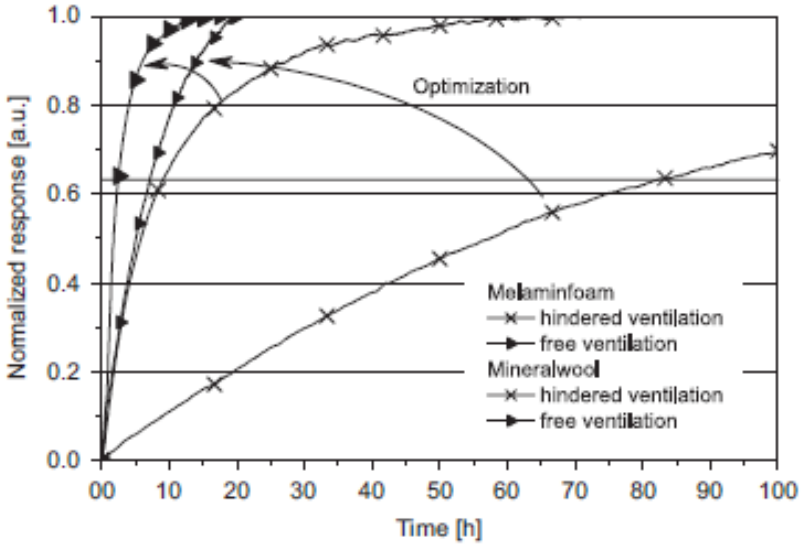

Figure 10: Impact of insulation materials in front of the ventilation openings on the humidity response function of collectors (Kohl et al, 2007,p. 725)

2-6 Simulation

It has been shown that ventilation rate and insulation materials are elements to determine the microclimatic condition. Simulation of the microclimate in solar thermal collectors helps in optimizing the collector. A computer program “MOMIC” (Modeling Of Microclimate In Collectors) was built to considered of the heat and moisture balance in the collector. The design tool helped to estimate the influence of ventilation of the collector (Holck et al. 2003).

Figure 11 shows the simulated humidity and the measured humidity for two days at a location in Denmark in April. The measured ambient weather data and the observed absorber temperature are used for the simulation of the humidity of the air in the air gap of the collector. From this, it is clear that there is a very strong correlation between the simulated and measured data. Very high wind speed was considered in order to investigate the influence of wind on the microclimate inside the collector. Figure 11 takes into account the effect of wind in the calculations, on the other hand, Figure 12 neglects it. One must take into account a windy period as this can cause disagreement of the measured and calculated data in Figure 12. These figures revealed that it is necessary to consider effects from wind to create a simulation. The ventilation is mainly caused by chimney effect, however, considering effects from wind makes the calculation more complex (Holck et al. 2003).

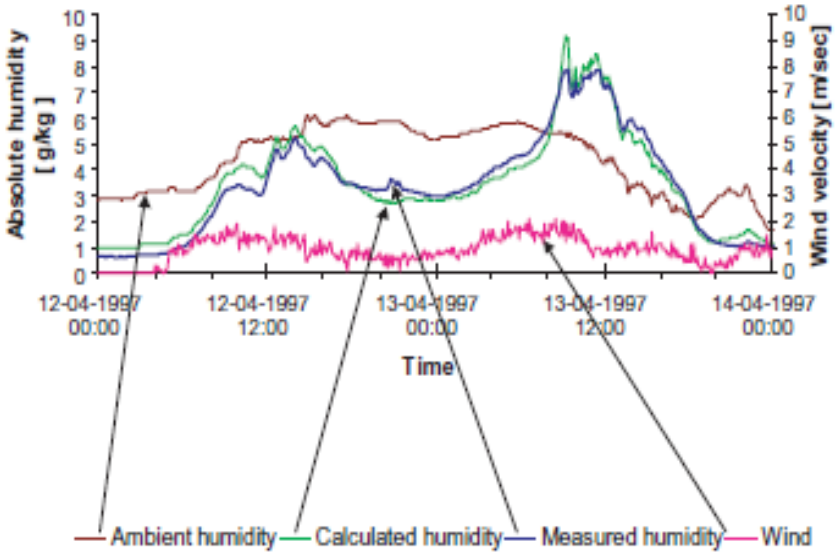

Figure 11: Measured and calculated humidity of the air in the air gap of the collector together with the ambient humidity and the wind velocity for two days in April (Kohl et al, 2003,p. 272)

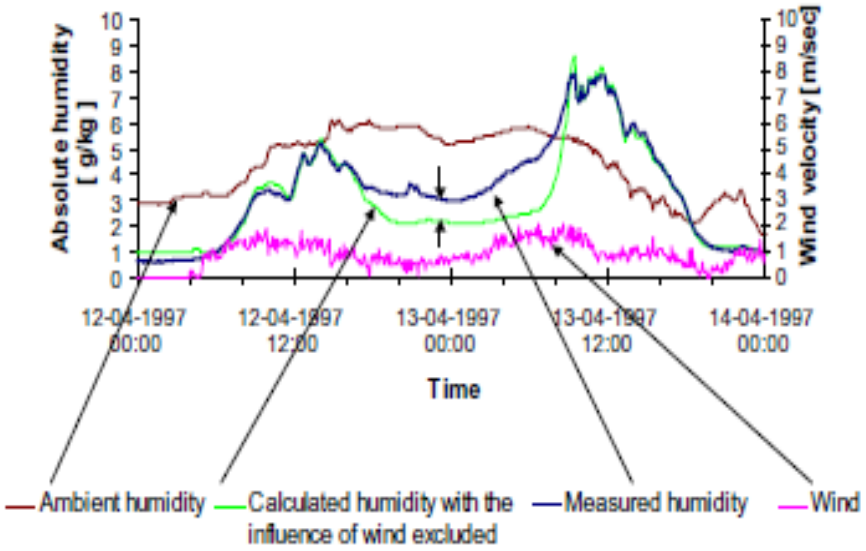

Figure 12: Humidity in the air gap. The calculations do not take into account the effect from wind. Ignoring the influence of wind leads to a disparity at night between the lines representing the measured and computed humidity (Kohl et al, 2003,p. 272)

Figure 13 displays the condensation on the inside of the cover for three collector designs, which are with a high ventilation rate at 300 $lh^{-1}Pa^{-1}$, a low ventilation rate at 40 $lh^{-1}Pa^{-1}$ including vapor barrier, and without a vapor barrier between the absorber and the insulation. Table 1 reviews the results in terms of the peak condensation levels and the time during which condensation occurs. Table 1 also highlights the cases with and without the vapor barrier as the existence of the barrier does not make significant difference in terms of the number of hours during which condensation is present. However, the total amount of condensation is decreased and there is no visible condensation. The case including a vapor barrier and a ventilation rate at 40 $lh^{-1}Pa^{-1}$ shows the smallest amount of condensation.

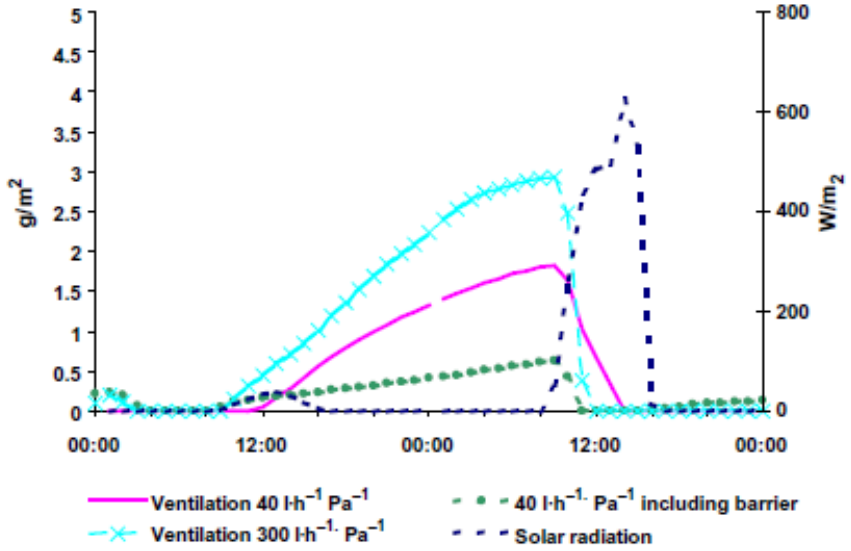

Figure 13: Calculations of condensation on the inner side of the cover are shown together with solar radiation for two days in January in the Northern hemisphere for different ventilation rates

(Kohl et al, 2003,p. 273)

Table 1 Condensation on the cover, calculated for two days in January

(Kohl et al, 2003,p. 273)

Condensation on the cover, calculated for two days in January

Ventilation rate ($l h^{-1}$)	Vapour barrier	Peak condensation ($g m^{-2}$)	Number of hours in the two days with condensation present on the cover	Number of hours in the two days with visible condensation present on the cover
40	Yes	0.6	26	0
40	No	1.8	26	14
300	No	2.9	27	23

To identify the microclimate, the accumulated appearance of time with condensation as well as the time with relative humidity attaining a certain level is presented as a function of the ventilation rate of the collector box. The result which is considered the ventilation rate of the solar collector box described in Figure 14 and Figure 15. The ventilation rate of the collector was changed in the range between 5 and 850 lh-1. Both figures show that humidity rises at a higher ventilation rate in the collector. The results for the calculations of the annual occurrence of condensation exceeding 1,2,4,6,8 and 10 gm-2 for the collector are presented in Figure 14. Low occurrence of high humidity and non-visible condensation up to 80 $lh^{-1}Pa^{-1}$ are shown with in Figure 14 and 15. In all cases the occurrence of condensation increases with higher rate of ventilation (Holck et al. 2003).

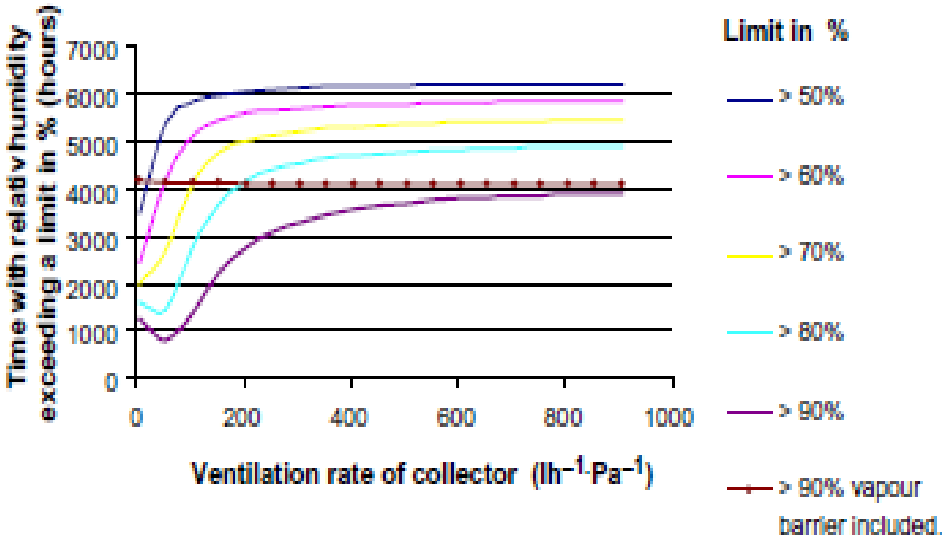

Figure14: Annual calculation of relative humidity showing the dependence of the ventilation rate of the collector (Kohl et al, 2003,p. 272)

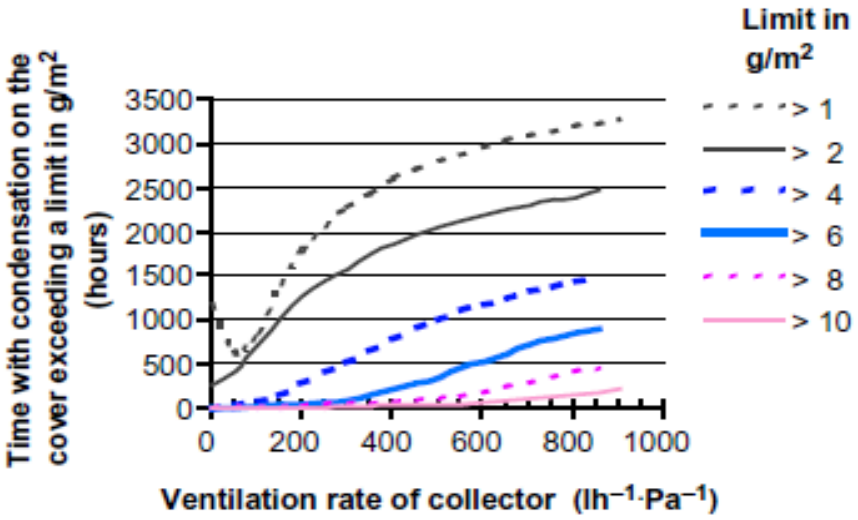

Figure 15: Annual calculations of condensation on the inner surface of the cover.

(Kohl et al, 2003,p. 274)

2-7 Statement of the research intent

It is important to prevent occurring condensation in solar collectors in terms of its durability and performance. During night periods solar collectors release heat to the atmosphere by radiation, this occurs condensation inside and outside the glazing especially when it's cold and humid. The existence of water not only damages the selective surface, it causes corrosion on the absorber plate, and means energy is wasted in evaporating the moisture during the next day.

This thesis's purpose is to develop a numerical model of the microclimate in the solar collector from first principles using weather data as the only input and, to validate the model with experiments. The microclimate will be using real weather data to understand how condensation affects collector performance, the frequency of condensation in flat plate solar collectors, and to reveal the factors that influence condensation.

Chapter 3: Methodology

This chapter presents the two methods used in this study: a numerical method and the experimental method. The numerical method was used to create the model of the microclimate inside a solar collector and to simulate it. Experiments were conducted to assess the performance of the model and, to compare the data from the model and actual data. This section details the process of creating the numerical model used to analyze the collector and explains the experimental method that was used to validate the model.

3-1 Modeling

The following sections focus on the parameters used to create the numerical model of the microclimate in the collector and describes the equations used to create the model. It consists of four elements; the heat balance, the rate of ventilation, wind and the humidity or moisture content inside the collector.

There are a number of software programs that could be used to create a computer model of a solar collector for this study, however, Microsoft Excel was chosen because of its flexibility and its ability to interactively solve linear and non-linear problems. Therefore the ‘Solver’ function was used to solve the energy balance, ventilation rate and moisture balance inside the collector.

To calculate the heat balance, there were several differential equations that needed to be solved. There are many methods to solve differential equations, however, the 4th order Runge -Kutta method were employed to solve the equations. The basic idea of the 4th order Runge-Kutta methods is to correct the predicted value of the slope and extrapolate the solution to the future time step in the numerical solution. The 4th order Runge-Kuetta algorithm was written in 'VBA (Visual Basic for Application)'and linked to Excel.

3-1-1 Heat balance

In the model, it was assumed that there was no difference in temperature between the corners and the center of the collector. The heat balance was developed with respect to a panel of unit area (ie, $1\,m^2$). It is assumed that the absorber contain half of the back insulation and the fluid. Figure 16 illustrates a cross sectional view of a single cover collector, where T_a is the ambient temperature, and T_i is the temperature inside the collector.

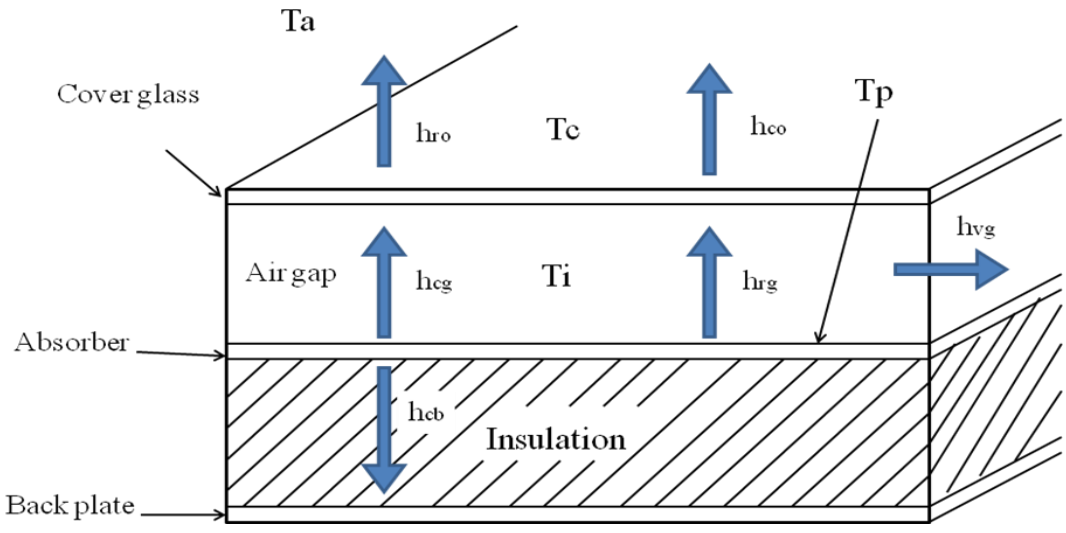

Figure 16: A cross sectional view of the collector

It is essential to calculate the heat transfer by convection and thermal radiation from all the surfaces and conduction in the solar collector. And those parameters are described by the heat transfer coefficient and the temperature difference. To determine the absorber and cover temperature, the heat balance equations (Equation (7) and (8)) need to be solved (Kohl, 2004).

$$C_p \frac{dT_p}{dt} = G(\tau\alpha) - h_{cb}(T_p - T_a) - h_{cg}(T_p - T_c) - h_{rg}(T_p - T_c) \quad (7)$$

$$C_c \frac{dT_c}{dt} = Ga_c + h_{cg}(T_p - T_c) + h_{rg}(T_p - T_c) - h_{vg}(\frac{T_p + T_c}{2} - T_a) - h_{co}(T_c - T_a) - h_{ro}(T_c - T_s) - q_{ei} - q_{eo} \quad (8)$$

In equations (7), (8), G is solar radiation from the sun (J). τ is the transmittance of the cover and α is the angular absorptance of the absorber plate. Generally, $\tau\alpha$ is called the transmission absorption product of the solar collector.

h_{cb} is the heat loss through the back insulation. h_{cg} and h_{rg} respectively represent the heat transfer coefficient for natural convection and thermal radiation in the air gap. h_{ro} is the heat transfer coefficient for thermal radiation from the cover to the ambient air. h_{co} is the heat transfer by convection from the cover to the ambient air. The heat transfer coefficient due to ventilation was expressed by h_{vg}. q_{ei} and q_{eo} are the heat transfer by evaporation and condensation.

The conductive heat loss through the back insulation material h_{cb} is given by a modified form of Fourier's law. (equation (9)) e_i is the thickness of the insulation.

$$h_{cb} = \frac{k_i}{e_i} \quad (9)$$

The convective heat transfer coefficient between the absorber and the glazing (h_{cg}) is expressed in terms of three parameters: the thermal conductivity of air (k_0), the thickness of the air gap (e_g) and the Nusselt number (Nu_g). The Nusselt number is a function of the slope of the collector, which has a significant influence on the performance of the collectors across the year. The heat transfer by natural convection h_{cg} is give by equation (10) (Kohl, 2004).

$$h_{cg} = \frac{Nu_g k_0}{e_g} \tag{10}$$

In equation (10), Nu_g is the ratio of convection to conduction in the air gap. Duffie et al. (1991) showed a correlation between the Nusselt number and Rayleigh number for tilt angles from 0 to 75° as expressed by equation (11) :

$$Nu_g = 1 + 1.44\left[1 - \frac{1708}{Ra_g \cos s}\right]^+ \left(1 - \frac{(\sin 1.8 \cdot s)^{1.6} \cdot 1708}{Ra_g \cos s}\right) + \left[\left(\frac{Ra_g \cos s}{5830}\right)^{0.33} - 1\right]^+ \tag{11}$$

In equation (11), the positive superscript indicates that if the values in the square brackets are negative, the values will be zero. Rayleigh number for air inside the collector is give by equation (12).

$$Ra_g = \Pr \cdot \frac{g\beta(T_p - T_c)e_g^3}{\nu^2} \tag{12}$$

Where β is volumetric coefficient of expansion of the air.

The approximation of β is given by equation (13)

$$\beta = \frac{2}{T_P + T_c} \tag{13}$$

The heat transfer radiation from the cover to the sky and to the surrounding ground (h_{ro}) is given by Equation (14). (Kohl, 2004)

$$h_{ro} = f_1(1+\cos s)\varepsilon_c C_s\left(\frac{T_c^4 - T_s^4}{T_c - T_s}\right) + f_2(1-\cos s)\varepsilon_c C_s\left(\frac{T_c^4 - T_a^4}{T_c - T_s}\right) \quad (14)$$

Where the view factor f_i to each is taken to be 0.5 and T_s is the sky temperature.

Duffie et al (2004) expressed the sky temperature using the dew point temperature and the time from midnight as shown in equation (6) from previous section.

$$T_s = T_a\left[0.711 + 0.0056T_{dp} + 0.000073T_{dp}^2 + 0.13\cos(15t)\right]^{\frac{1}{4}} \quad (6)$$

Where T_s and T_a are in Kelvin and T_{dp} is the dew point temperature in degrees Celsius, and t is the number of hours from midnight. The equation (6) is effective for a dew point from -20℃ to 30℃ and clear sky conditions, however, it was assumed to be valid for any conditions.

The heat transfer by convection from the cover to the ambient air can be expressed by equation (15).

$$h_{co} = Nu_0 \frac{k_g}{L} \quad (15)$$

The Nusselt number for convection (Nu_0) is calculated from the square root of the Nusselt number for laminar flow and turbulent flow as shown in equation (16). The Nusselt number is given as a function of Reynolds number and Prandtl number for laminar and turbulent flow as shown in equation (17) and (18) (Kohl, 2004).

$$Nu_0 = \sqrt{Nu_{lam}^2 + Nu_{tur}^2} \quad (16)$$

$$Nu_{lam} = 0.664\,\mathrm{Re}_{+}^{0.5}\,\mathrm{Pr}^{0.33} \tag{17}$$

$$Nu_{turb} = \frac{0.037\,\mathrm{Re}_{+}^{0.81}\,\mathrm{Pr}^{0.33}}{\left(1 + 2.443\,\mathrm{Re}_{+}^{-0.1}(\mathrm{Pr}^{0.67} - 1\right)} \tag{18}$$

The Reynolds number (*Re*) is a dimensionless number representing the ratio of inertial forces to viscous forces. In equation (19) the overall Reynolds number Re_{+} is taken to be the sum of a forced and free component (Kohl, 2004).

$$\mathrm{Re}_{+} = \sqrt{\mathrm{Re}^2 + \mathrm{Re}'^2} \tag{19}$$

The Reynolds number for forced flow *Re* on the cover of the collector can be determined from three elements : wind speed (Vw), kinematic viscosity (v) and characteristic length (L) as shown in equation (20) (Kohl, 2004).

$$\mathrm{Re} = Vw\frac{L}{v} \tag{20}$$

The Reynolds number (Re') for natural convection by defining an equivalent Reynolds number is given by equation (21) (Kreith, 1973).

$$\mathrm{Re}' = f(\mathrm{Pr})Gr^{0.5} \tag{21}$$

Where $f(\mathrm{Pr})$ is the function for air.

$f(\mathrm{Pr})$ depends on the Prandtl number. Kreith (1973) analyzed 0.64 was used as a best fit equivalent Reynolds number for natural convection as shown in equation (22) (Kreith, 1973).

$$\mathrm{Re}' = 0.64Gr^{0.5} \tag{22}$$

In equation (22) the Grashof number (Gr) is a nondimensional parameter used to quantify the heat transfer due to natural convection and between the cover and the ambient air. Gr is given by equation (23) (Kohl, 2004).

$$Gr_L = L^3 \cdot g \cdot \beta \frac{(T_S - T_\infty)}{v^2} \tag{23}$$

Where T_S : Surface temperature, T_∞ Bulk temperature, and $\beta = \frac{2}{T_a + T_c}$

Rearranging equation (23) gives equation (24) (Kohl, 2004).

$$Gr = 2 \cdot L^3 \cdot g \frac{(T_c - T_a)}{v^2 (T_a + T_c)} \tag{24}$$

The heat transfer by condensation and evaporation of moisture at the outer cover is expressed by equation (25) and (26). Condensation occurs if the cover temperature falls below the dew point temperature. Equations (25) and (26) can be used only for condensation, however, it was assumed that it is valid for evaporation even though evaporation takes place when only the cover is wet (Kohl, 2004).

$$T_c \geq 0 : q_{eo} = 0.017 \cdot h_{co} \{p_{ws}(T_c) - p(T_{dewa})\} \tag{25}$$

$$T_c \leq 0 : q_{eo} = 0.019 \cdot h_{co} \{p_{ws}(T_c) - p(T_{dewa})\} \tag{26}$$

Where T_c is the cover temperature and T_{dewa} is the dew point temperature

To determine the dew point temperature from the weather data, normally a psychometric chart is applied. A psychometric chart is a graph which describes the thermodynamic parameters of moist air. Figure 17 shows a sample of psychometric charts. During the simulation, the dew point was collected from the National Institute of Water and Atmospheric Research's (NIWA) Cliflo database (NIWA, 2010).

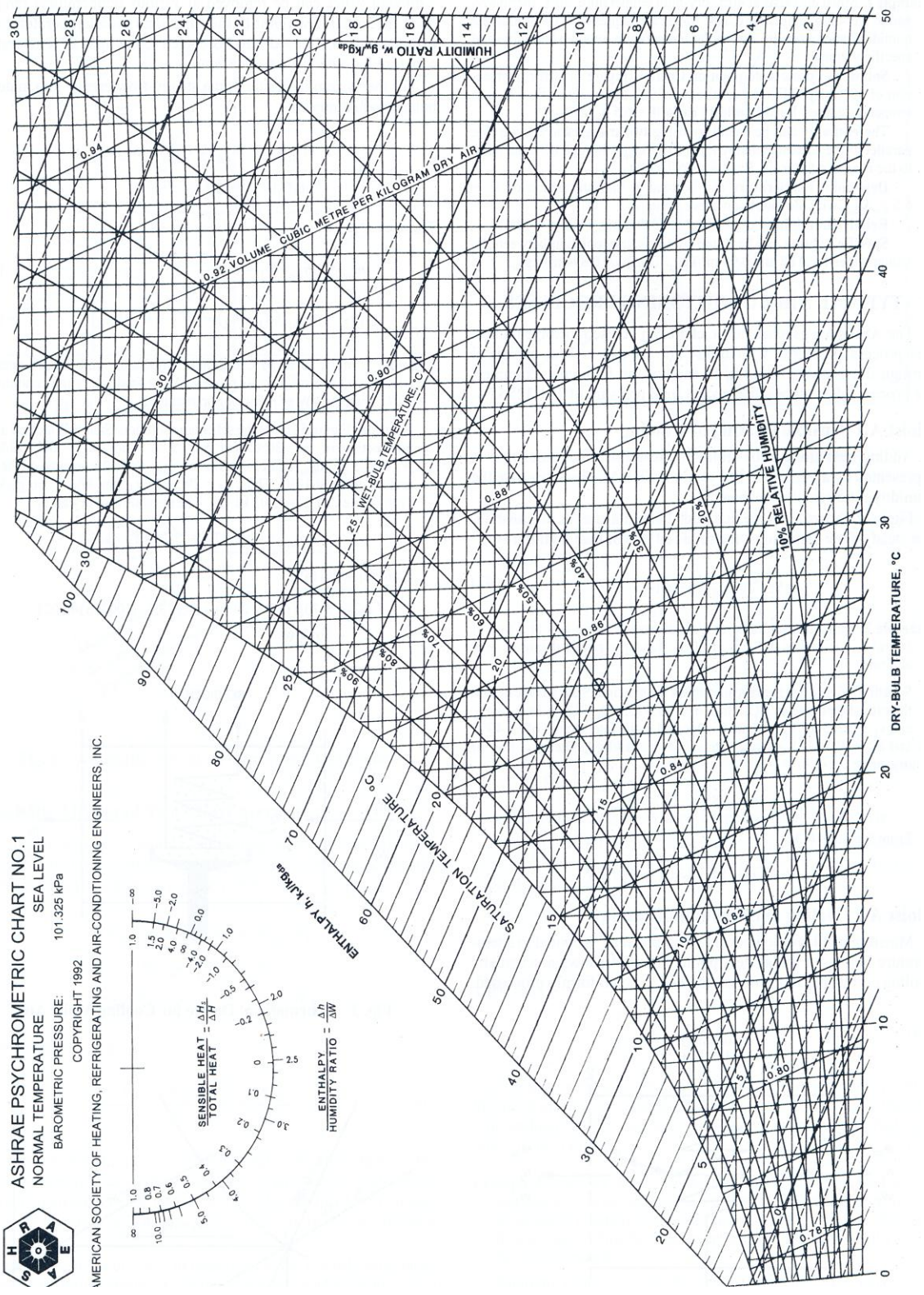

Figure 17: A sample of the psychometric chart (ASHRAE 2009, p. 1-11)

The evaporation heat loss from the inside of the cover q_{ei} is expressed by the mass transfer rate of air through the air gap and the latent heat of water. The equation (27) shows heat transfer by evaporation or condensation at the inside of the cover (Duffie, 2004).

$$q_{ei} = m_{vg} h_{fg} \tag{27}$$

The heat transfer coefficient because of ventilation (h_{vg}) is obtained from equation (28) (Kohl, 2004).

$$h_{vg} = m_{vg} C_{pa} \tag{28}$$

The thermal radiation between two parallel plates, the radiation can be expressed as (29) (Duffie, 2004).

$$Q = \frac{C_s (T_p^4 - T_c^4)}{\frac{1-\varepsilon_p}{\varepsilon_p A_p} + \frac{1}{A_p F_{12}} + \frac{1-\varepsilon_c}{\varepsilon_c A_c}} \tag{29}$$

Where F_{12} is a view factor, ε_p is the absorber emissivity, ε_c is the cover emissivity and C_s is the Stefan-Boltzmann constant.

If it is assumed that the areas A_c and A_p are equal and the view factor F_{12} is unity. The equation (29) simplifies to be equation (30).

$$Q = \frac{C_s (T_p^4 - T_c^4)}{(\frac{1}{\varepsilon_p} + \frac{1}{\varepsilon_c} - 1)} \tag{30}$$

From equation (30), the convection coefficient for thermal radiation between two parallel plates can then be given by equation (31).

$$h_{rg} = \frac{C_s(T_p^4 - T_c^4)}{(\frac{1}{\varepsilon_p} + \frac{1}{\varepsilon_c} - 1)(T_p - T_c)} \quad (31)$$

3-1-2 Ventilation

The ventilation in solar collectors referred to in equation (28) is caused by a number of factors: thermal driven pressure (the stack effect), actual heating and cooling of the solar collector, constant wind and pumping effects.

Due to the difference of temperature in air at the bottom and top, the solar collector will cause ventilation (the stack effect). The actual heating and cooling in the solar panel will also cause ventilation. As wind passes over the solar collector, the wind induces a pressure difference between collector and the surroundings causing air flow through gaps and cracks in the collector. The pumping effect is caused by positive pressure ventilation, it increases output. Ventilation which includes all elements is overly complex to model, so only thermal driven pressure is considered in this model.

The driving pressure is the pressure difference caused by the pressure loss of the distance from the neutral plane. The driving pressure is given by the density of the air, the gravity and vertical co-ordinate measured from the neutral plane (Kohl, 2004).

$$\Delta P = \Delta \rho g z = \left(\frac{273}{T_a} - \frac{273}{T_i} \right) g z \tag{32}$$

When the humidity of air is considered, the differential pressure is give by equation (33) (Kohl, 2004).

$$\Delta P = \left(\rho(T_a, P_{wa}) - \rho\left(\frac{T_p + T_c}{2}, P_{wg} \right) \right) h \cdot g \tag{33}$$

Where, P_{wa} is partial pressure of water in the open air and P_{wg} is partial pressure of water in the air of the air gap.

Moist air density (ρ_a) is defined as the reciprocal of the moist air specific volume (V). The density of the moist air density is calculated as shown in equation (34) (Kohl, 2004).

$$\rho_a = \frac{1}{V} \tag{34}$$

The specific volume of the moist air is expressed as equation (35) (Kohl, 2004).

$$V = \frac{R_a T}{p}(1 + 1.6078W) \tag{35}$$

And the humidity ratio of moist air (W) is defined by equation (36). (Kohl, 2004)

$$W = 0.62198 \frac{p_w}{p - p_w} \tag{36}$$

The mass flow of damp air is given equation (37) (Kohl, 2004).

$$m_{vg} = 0.5 \left(\rho(T_a, P_{wa}) + \rho\left(\frac{T_a + T_c}{2}, P_{wg} \right) \right) V \cdot \Delta P \tag{37}$$

Where ρ mean value is used for the density of the air. During the simulation, it is assumed that the pressure was equal both inside and outside the collector.

3-1-3 Wind

Knowledge of the actual wind velocity is important in order to calculate the heat transfer by convection from the cover to the ambient air. (Equation (20)) Wind shear influences the wind speed and, is related to the height. The wind speed on the surface is zero if it is assumed that there is no slippage on the surface, in other words, wind speed is zero at the height of zero. There are two ways to describe shear which are Power law profile and logarithm profile. Equation (38) is widely used to express the correlation of wind speed and height (Pramod 2011).

$$\frac{v_2}{v_1} = \left(\frac{h_2}{h_1}\right)^{\gamma} \tag{38}$$

Where v_2 and v_1 are wind speeds at heights h_2 and h_1, exponent γ is wind shear. The other method to extrapolate wind speed is applied the long arithmic profile which represents roughness of the surface.

$$\frac{v_2}{v_1} = \frac{\ln(h_2 / z_0)}{\ln(h_1 / z_0)} \tag{39}$$

Where z_0 is called the roughness length. If wind speed v_1 is available at h_1=10m, then the equation (39) is used to calculate v_2.

From equation (38) and (39), the value of shear can be described by equation (40).

$$\frac{v_2}{v_1} = \frac{\ln(\ln(h_2 / z_0) / \ln(h_1 / z_0))}{\ln(h_2 / h_1)} \quad (40)$$

As shown, equation (39) and (40) shear depends on the heights and roughness. At the surface, the mean wind speed can be assumed to be zero, so the wind speed has a logarithmic form. Table 2 shows typical values of roughness classes, Roughness Length, and shear.

Table 2: Description of Roughness classes, Roughness Length, and shear

Description	Roughness class	Roughness Length (m)	shear
Open sea	0	0.0001-0.003	0.08
Open terrain with a smooth surface, like concrete runway, mowed grass	0.5	0.0024	0.11
Open agricultural area without fences and hedgerows and very scattered buildings. Only softly rounded hills	1	0.03	0.15
Agricultural land with some houses and 8-m tall sheltering hedgerows with a distance of approx. 1250 m	1.5	0.055	0.17
Agricultural land with some houses and 8-m tall sheltering hedgerows with a distance of approx. 500 m	2	0.1	0.19
Agricultural land with some houses and 8-m tall sheltering hedgerows with a distance of approx. 250 m	2.5	0.2	0.21
Villages, small towns, agricultural land with many or tall sheltering hedgerows with a distance of approx. 250 m	3	0.4	0.25
Large cities with tall buildings	3.5	0.8	0.31
Very large cities with tall buildings and skyscrapers	4	1.6	0.39

Source: (Pramod 2011 Wind energy engineering P35)

3-1-4 Moisture balance

From the previous section 3-1-1, the temperature inside the collector was obtained. It was assumed that the volume of the collector was constant, and then Charles's law and Boyle's law are used to calculate the pressure in the collector (Equation (41)).

$$\frac{P_a}{T_a} = \frac{P_c}{T_i} \tag{41}$$

Where P_a atmospheric pressure in open air, P_c pressure inside the collector (Equation (42).

$$P_c = P_{ca} + P_{cw} \tag{42}$$

where P_{ca} is partial pressure of dry air inside the collector P_{cw} partial pressure of water vapor inside the collector

The absolute humidty of moist air (W) $(kg\ H_2O / kg\ dry\ air)$ is defined as the ratio of the mass of the water vapor (m_w) to the mass of the dry air (m_{da}) as shown in equation (43).

$$w = \frac{m_w}{m_{da}} \tag{43}$$

The moisture inside the collector is shown in equation (44).

$$W_i = 0.62198 \frac{P_{cw}}{P_c - P_{cw}} \tag{44}$$

Any moisture in the insulation was ignored and, the saturated vapor pressure inside of the collector (P_{cw}) was assumed to be equal to the saturated vapor pressure outside. The saturated vapor pressure outside was calculated from relative humidity outside.

When running the simulation, the weather data was used from The NIWA Cliflo database (NIWA, 2010). All weather data was written and organized in one Excel sheet, and transferred to another Excel sheet to calculate the absorber and cover temperatures. The 'Visual Basic for Application' (VBA) was used to transfer the weather data from one Excel sheet to another Excel sheet.

3-2 Experiment

To validate and assess the numerical model, an experiment to measure the absorber temperature, cover temperature and relative humidity in the air gap was conducted. A collector 1 meter long and 1.8 meters wide was positioned on the roof of AUT's WS building facing due north. The collector was inclined at an angle of 37° to the horizontal (Figure 18). The detailed collector characteristics are shown in Table 3.

Table 3: The experiment collector characteristics

The height of the collector	1	(m)
The width of the collector	1.8	(m)
Slope of the collector	37	(degrees)
Volume of the gap	0.015	(m^3/m^2)
Height of the collector (above roof)	2	(m)
The thickness of insulation	0.03	(m)
Thickness of the air gap	0.015	(m)

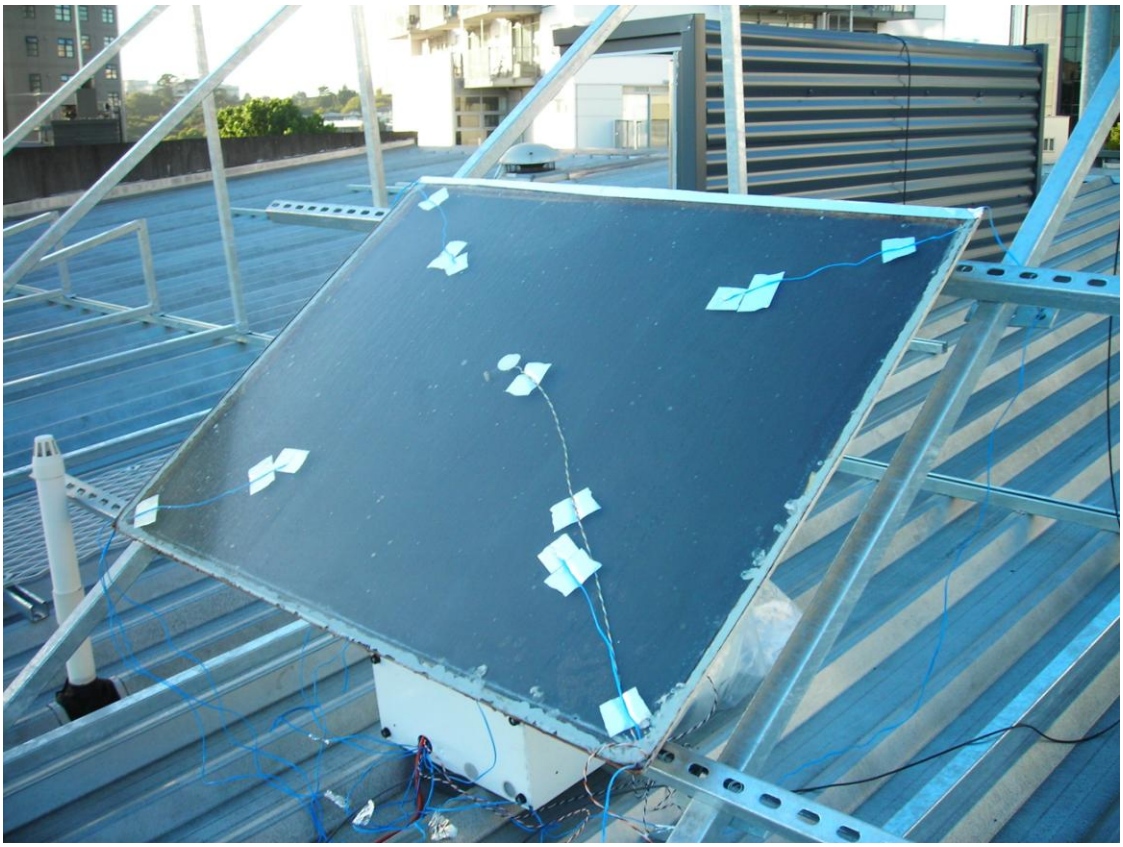

Figure 18: The flat plate solar collector used for the experiment

The collector was fitted with nine T-type thermocouple (±0.3℃). The first four thermocouples were attached to the surface of absorber, another 4 thermocouples were attached to the inside surface of the cover (Figure 19), the last thermocouple was used to measure the ambient temperature. The sensors for absorber and cover were uniformly distributed on the absorber and cover surface to determine the mean temperatures.

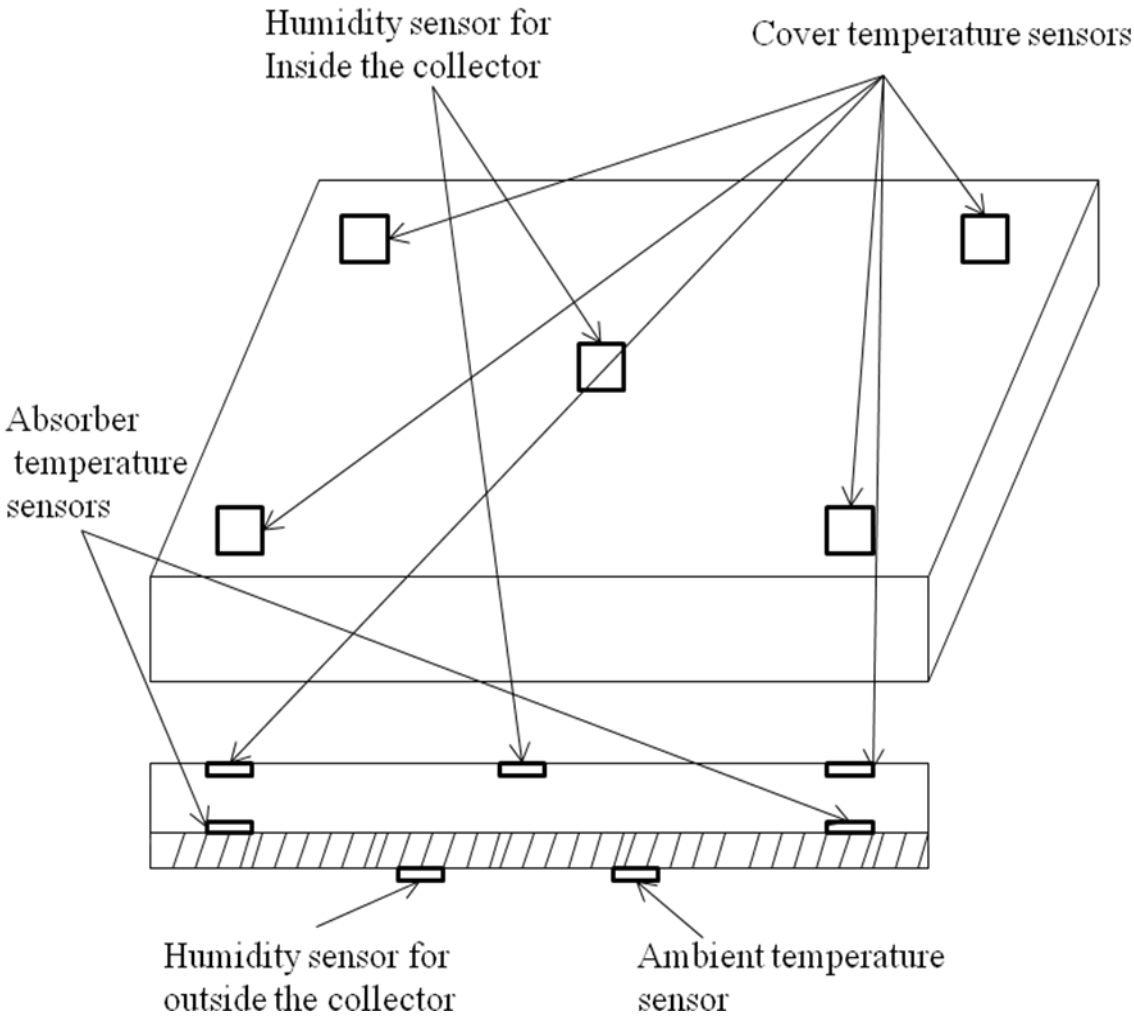

Figure 19: The positions of a humidity sensor and temperature sensors

In addition, two relative humidity sensors (Honeywell, HIH-4000) were used. A sensor was placed inside the collector air gap and the other in the ambient air to record the difference between relative humidity inside and outside the collector.

A pyranometer (Apogee, SP110) was used to measure the global radiation incident the collector. Atmospheric pressure was logged separately by the AUT weather data server. (http://weather.aut.ac.nz/weather/ServletTest.html).

To record the temperature, humidity and radiation data, an Agilent 34972 produced by Agilent technologies was used. The data was recorded at ten minute intervals and saved in an Excel sheet, to allow comparison with the simulated data.

Chapter 4: Results

4-1 Experimental Results

4-1-1 Temperature analysis

In the experiment, the ambient, absorber and cover temperatures, radiation, wind velocity and relative humidity inside and outside the collector were measured. Figure 20 shows the observed radiation, ambient temperature and wind velocity from a typical test. The radiation increased after sunrise, and reached the maximum around 2 pm, and the wind velocity was relatively strong especially during the day time.

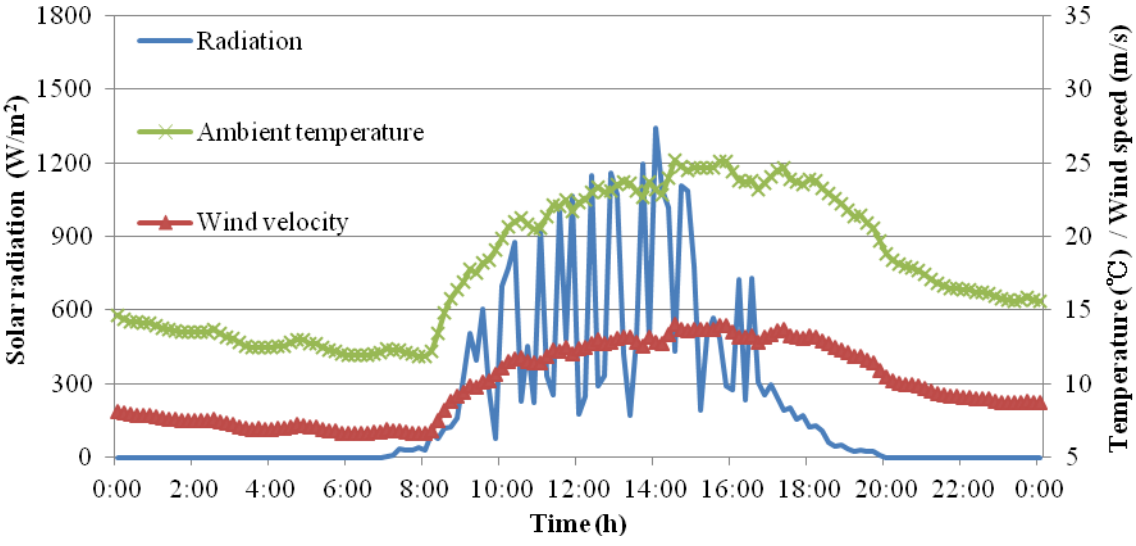

Figure 20: Measured radiation, ambient temperature and wind velocity in Auckland

In the experiment, thermocouples were uniformly distributed on the surface of the absorber and the inside of the cover, however, there was no significant difference between sensors. Figure 21 shows the measured absorber and cover temperature that was collected from the experiment. The absorber temperature reached approximately 100 ℃ while the cover temperature increased to 50℃ in the day time.

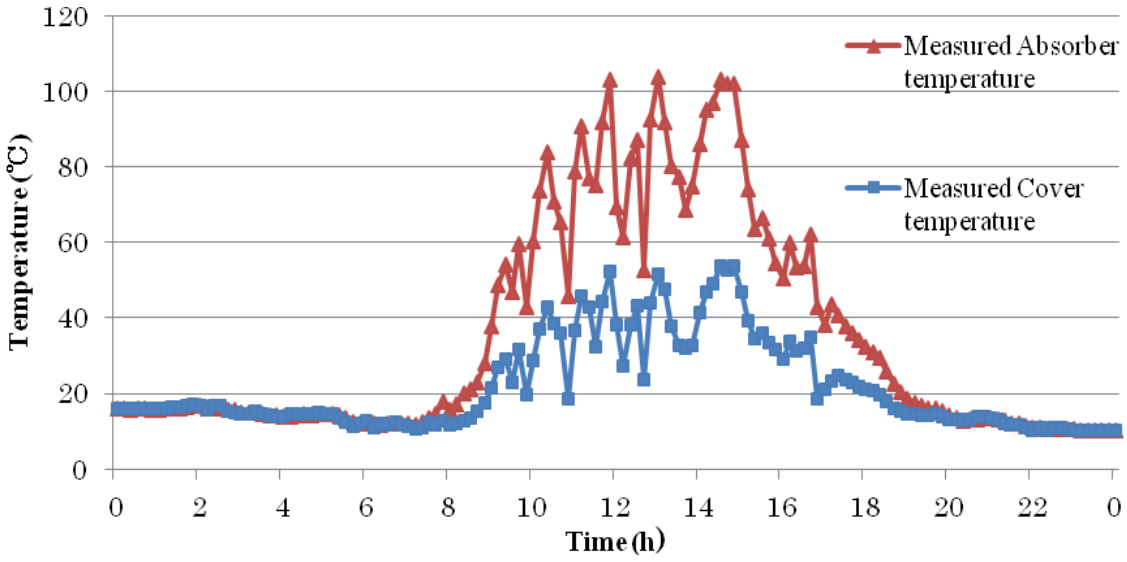

Figure 21: Measured absorber and cover temperature in Auckland

4-1-2 Humidity analysis

Figure 22 shows the measured relative humidity inside and outside of the collector for the test conditions. The relative humidity inside the collector changed considerably compared to the relative humidity outside of the collector. Relative humidity inside of the collector dropped after the sun came up and increased again after sunset. This shows that relative humidity inside of the solar collector behaves differently from that of the surrounding area, and that a microclimate exists in the solar collector.

The relative humidity inside the collector behaved as shown in Figure 22 because the temperature inside the collector increased as solar radiation increased. Even though the absolute humidity inside does not necessarily change, the amount of saturated vapor relative to dry air changes. For this reason, the relative humidity inside the collector goes down during the day time.

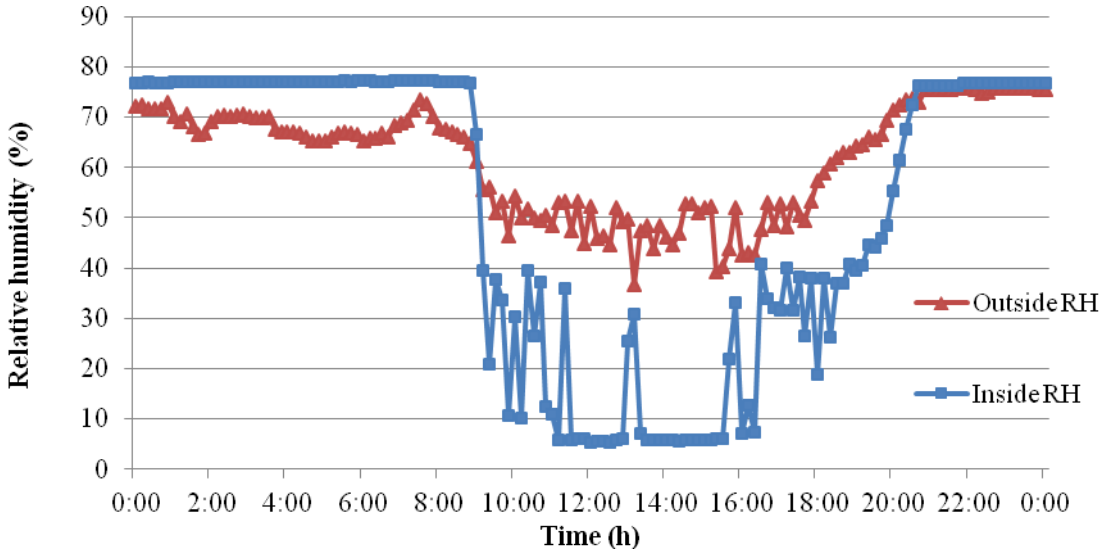

Figure 22: Measured relative humidity, inside and outside of the collector

In Figure 22, there is a modest difference between inside and outside relative humidity in the morning compare to at night. In the early morning, the difference was around 5%, but after 8 pm the difference was only 2 or 3%. The possible reason might be the difference of the wind speed, because in Figure 20 in the moring the wind speed was slower than at night, so the inside collector might have been closer to stagnation condition in the morning.

4-2 Model validation

4-2-1 Comparison between measured and simulated data

To examine the model, the results of experiment and the simulation were compared. The design characteristics of the collector model were input as shown in Table 4. The parameters were the same as the collector which was used in the experiment. However several parameters, such as characteristic length, emissivity of the cover and absorber, the coefficient of ambient air and back insulation, and Prandtl number were assumed.

Table 4: The simulation collector characteristics

Slope of the collector	37	(degrees)
Volume of the gap	0.015	(m^3/m^2)
Height of the collector	2	(m)
Emissivity of the cover	0.9	
Emissivity of the absorber	0.8	
The thickness of insulation	0.03	(m)
Thickness of the air gap	0.015	(m)
Characteristic length	1	(m)
The coefficient of thermal conduction	0.04	(W/mK)
The coefficient of the ambient air	0.0257	(W/m℃)
Prandtl number for the air	0.713	

In Figure 23, the measured absorber temperature was compared with the simulated absorber temperature. The absorber temperature fluctuations are the result of the variation in the incident radiation as seen in Figure 20. However, it can be seen that the simulation was able to predict the absorber temperature relatively well, especially at night when condensation might occur. In Figure 24, the measured and simulated cover temperature are compared, the simulated cover temperature showed almost the same temperature as the measured cover temperature.

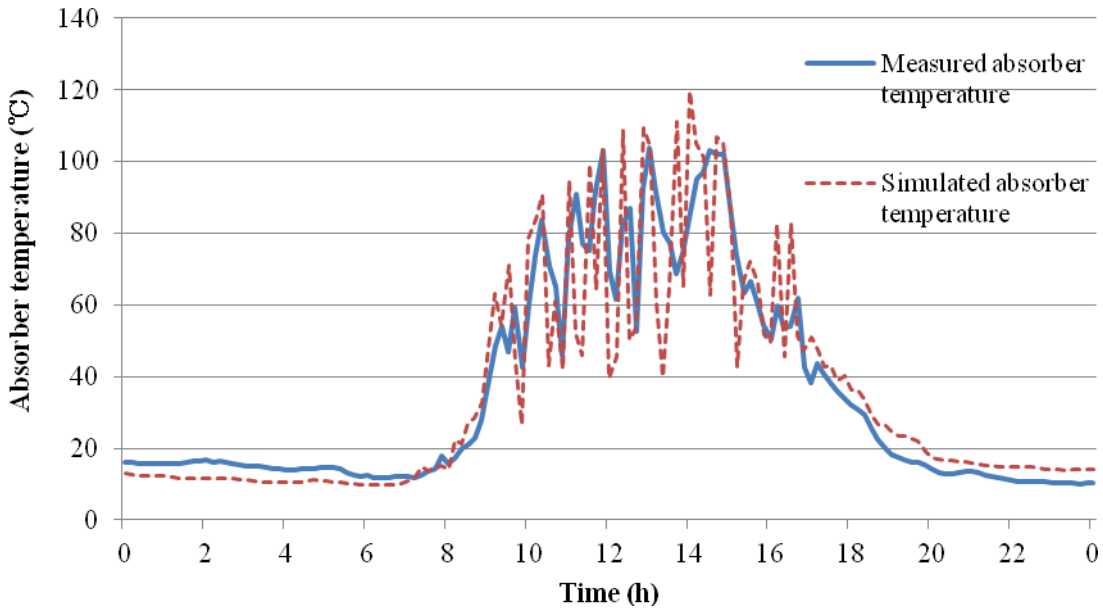

Figure 23: Measured and simulated absorber temperatures

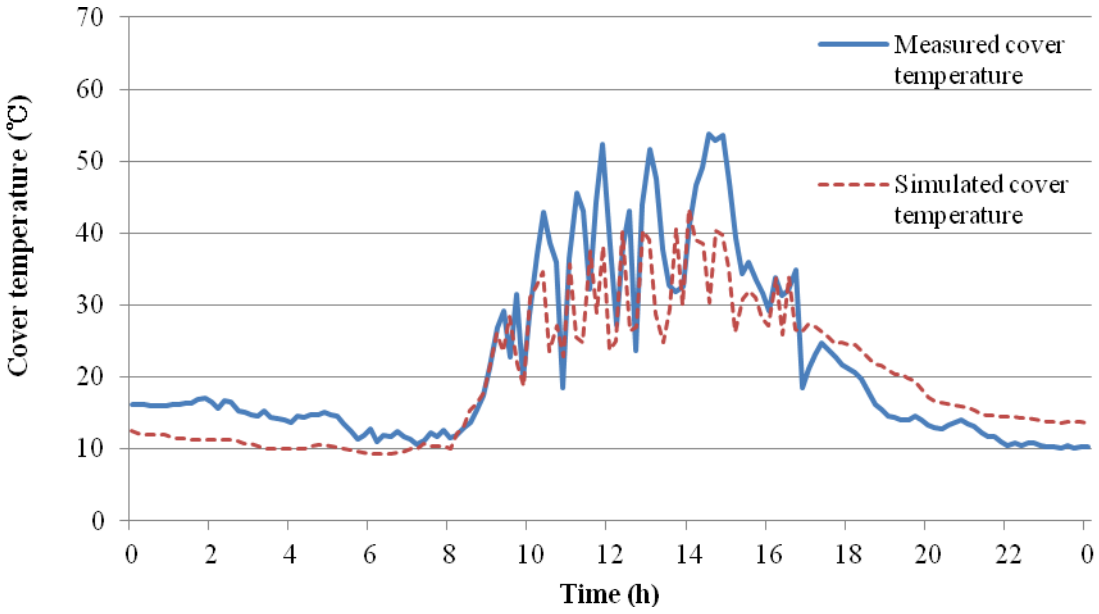

Figure 24: Measured and simulated cover temperatures

In Figure 25 measured and simulated relative humidity in the air gap with respect to the relative humidity in the collector are compared. It can be seen that there is a minor difference between simulated and measured relative humidity. However, the simulated relative humidity shows the same trend as measured data, in that it dropped around 9am as the sun went up and increased after 6pm as the sun went down. It could be said that simulated relative humidity can predict a change of relative humidity inside of the collector. In Figure 25, in the morning and at night, there is a small difference between measured humidity and simulated humidity. The possible reason why there are some minor errors between measured and simulated humidity is that during the calculation the water vapor pressure was assumed to be same as water vapor pressure in open air.

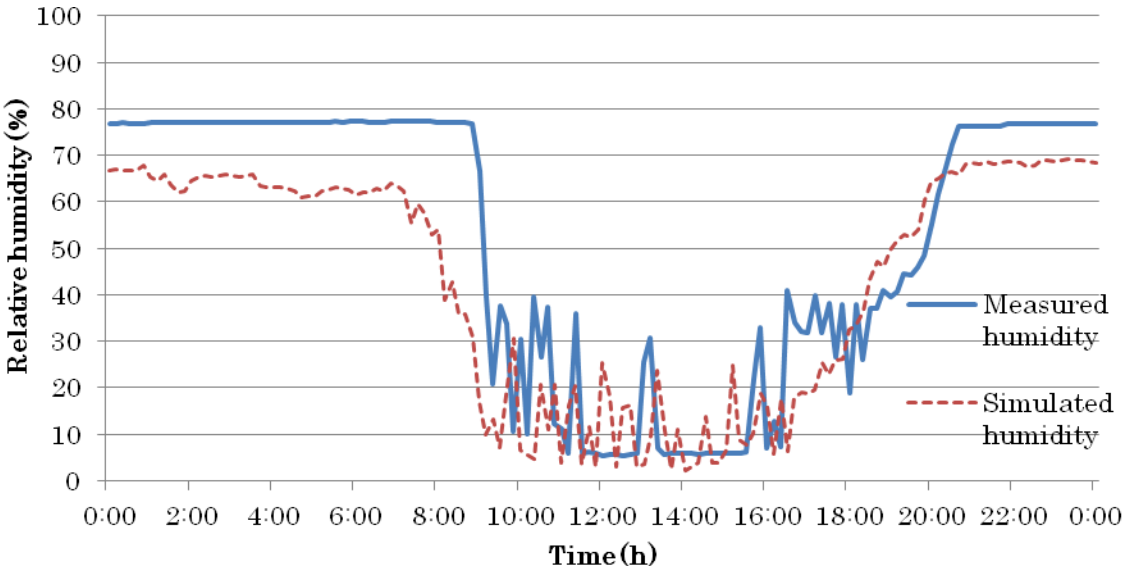

Figure 25: Measured and simulated relative humidity insde the collector

4-2-2 Verification test

During the experiment, a verification test was carried out to test the model's ability to predict the occurrence of condensation. Some moisture was found on the collector at 8am on 22nd of March as shown in Figure 26.

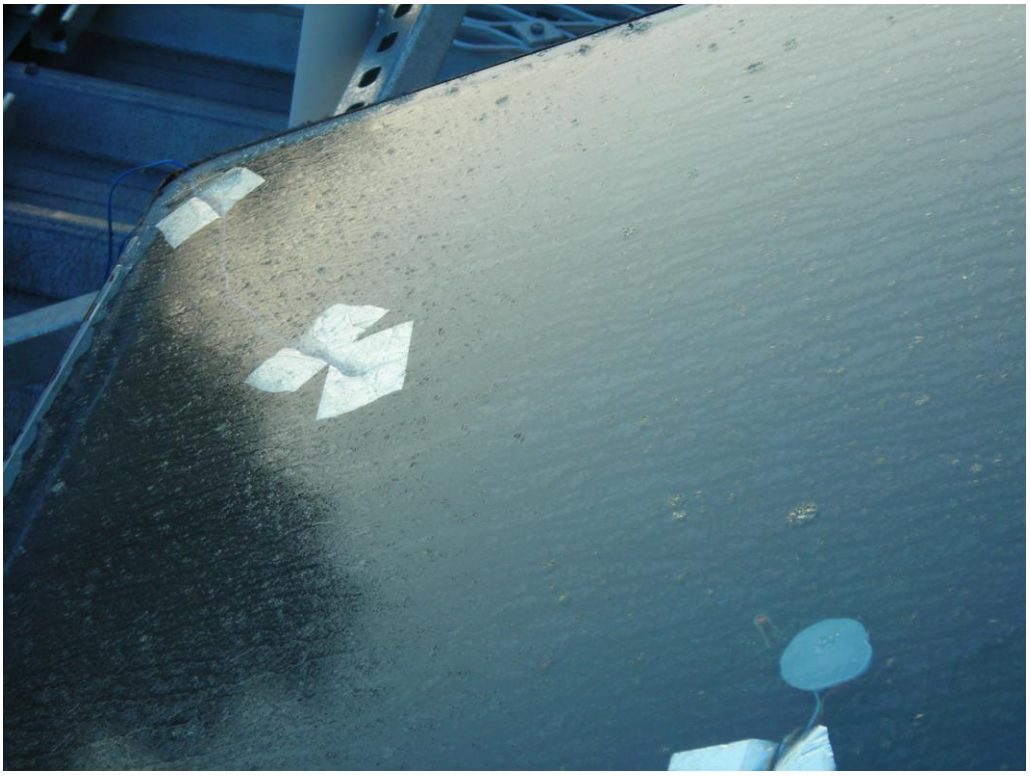

Figure 26: Condensastion on the collector on top of the roof

Therefore a simlulation was conducted using data collected from the NIWA Cliflo database (NIWA, 2012). Figure 27 shows the simulated absorber, cover temperature and the dew point temperature from NIWA Cliflo database. From the simulation, if it is assumed that condensation occurs on the surfce of the collector when the cover temperature is lower than the dewpoint temperature, condensation could occur until 7:30am.

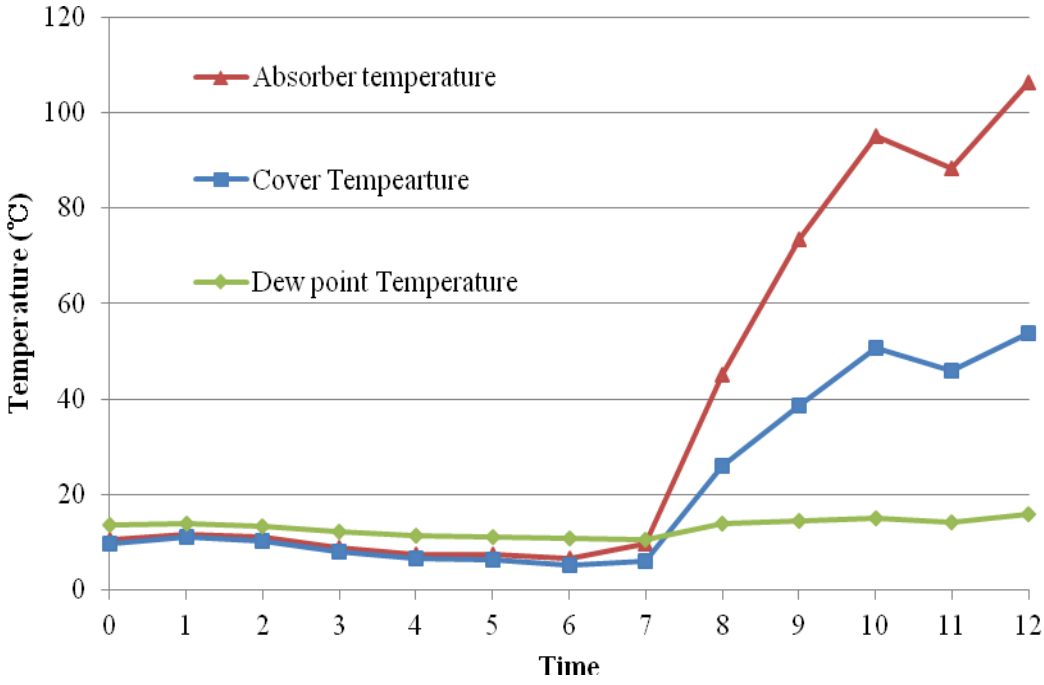

Figure 27: Simulated absorber, cover temperature and dew point temperature from NIWA

Because the weather information from the NIWA Cliflo database was collected and applied to the simulation, the location was not exactly the same as the test site. Therefore, the condensation persisted slightly longer than the model predicted. However, the model helped to predict the occurrence of condensation on the collector and provided a relatively accurate prediction of its duration.

4-3 Sensitivity analysis

During the simulations, a collector with the design characteristics as shown in Table 5 was modeled. The absorber plate and tubes were assumed to be copper and that condensation occurs when the cover temperature falls the dew point temperature.

Table 5: A collector characteristics for the simulation

Slope of the collector	30	(degrees)
Volume of the gap	0.015	(m^3/m^2)
Height of the collector (above the ground)	5	(m)
Emissivity of the cover	0.9	
Emissivity of the absorber	0.8	
The thickness of insulation	0.05	(m)
Thickness of the air gap	0.025	(m)
Characteristic length	1	(m)
The coefficient of thermal conduction	0.04	(W/mK)
The coefficient of the ambient air	0.0257	(W/m℃)
Prandtl number for the air	0.713	

To better understand the factors that influence the frequency of condensation in New Zealand solar collectors, the following parameters were changed : 1, Location 2, Emissivity of the cover 3, Emissivity of the absorber 4, Collector slope 5, Insulation thickness 6, Ventilation rate 7, Thickness of the air gap

4-3-1 Influence of location on condensation frequency

The model was tested by using weather data for Auckland, Hamilton, Wellington, Christchurch and Dunedin in New Zealand for the year 2010. The weather data was collected from the NIWA Cliflo database (NIWA, 2012).

Figure 28 shows the simulated absorber and cover temperature and the measured ambient and dew point temperature in Auckland on a typical winter day. This graph indicates that condensation may have taken place from midnight to approximately 8:30 am, and 6 pm to midnight since the cover temperature was lower than the dew point temperature.

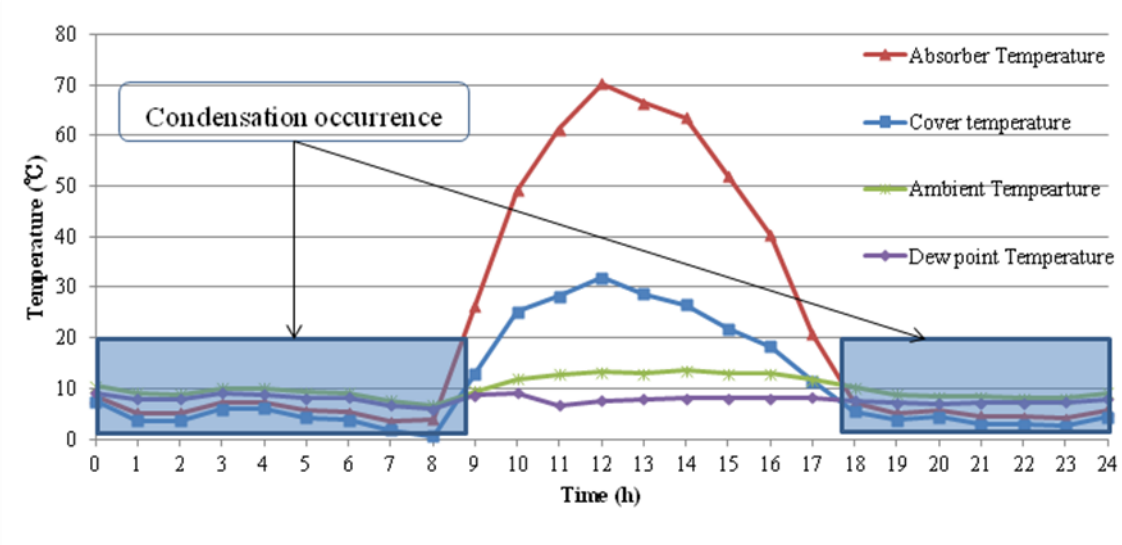

Figure 28: Simulated absorber and cover temperatures and ambient, dew point temperature from NIWA on a typical winter day in Auckland

The frequency of annual condesation in Auckland, Hamilton, Welington, Christchurch and Dunedin were simulated and, compared. In Figure 29, it is showed the simulated total amount of condensation time in each month for 2010 for each city. In Figure 29, it can be seen that in the winter season condensation would be expected to occur more than in the summer season in any location.

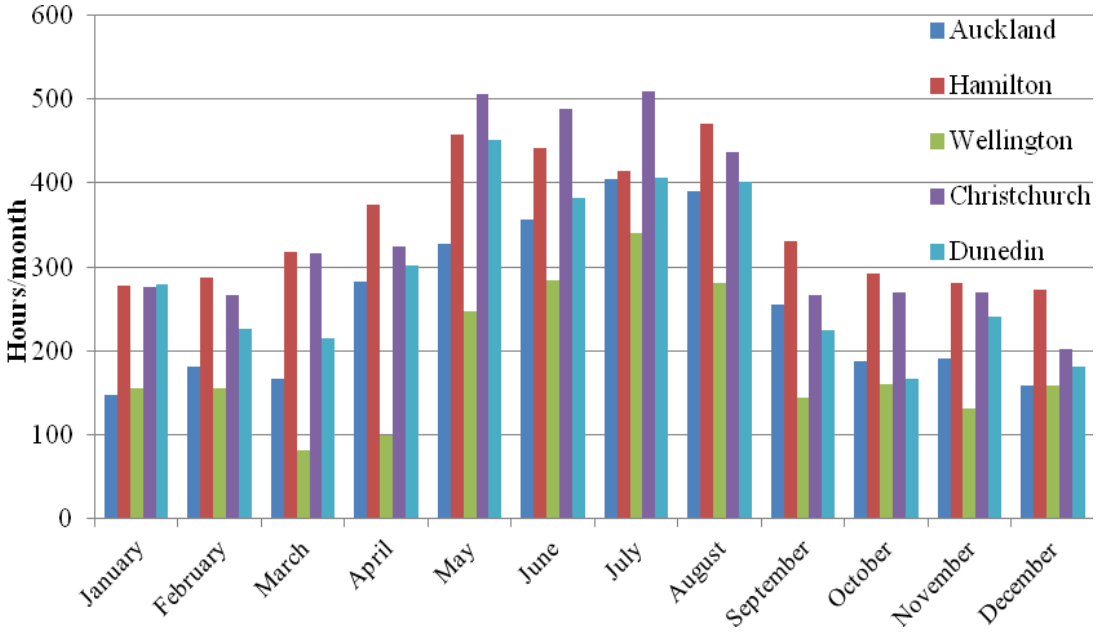

Figure 29: Expected monthly condensation hours in Auckland, Hamilton, Wellington, Christchurch and Dunedin for 2010

In Auckland, the annual condensation hours on the surface of the collector were expected to be 3049 hours. The simulated total amount of condensation time in winter reached more than double that in the summer season.

In Hamilton, the predicited annual condensation was found to be 4215 hours, which was significantly higher than Auckland. It was expected that the number condensation hours in Hamilton would be higher than Auckland because the climate in Hamilton is temperate and humid due to the greater number of small lakes and swamps. Typically, summers are warm and dry, on the other hand, winters are cool and wet and it has the lowest wind speed averages for a city in New Zealand because it is located inland and low altitude.

According to NIWA, in 2010, in Hamilton the average wind speed was 2.8 m/s which is quite low and, the relative humidity was 80 % which is relatively high (NIWA, 2010). As a result, the frequency of condensation hours in Hamilton was significantly higher than the other places, and it was discovered that climatic factors including relative humidity and wind speed play a significant role in the occurrence of condensation on a surface of the collector.

The simulation was also conducted for Wellington in 2010. The annual simulated condensation hours in Wellington were 2242 hours which was considerably lower than Auckland. Wellington is famous for its southerly blasts in winter that make the temperature feel colder, the city is generally very windy all year. The average wind speed in Welington was approximately 6.9 m/s which was significantly faster than the wind speed in Auckland (NIWA, 2010). As a result, the frequency of condensation hours in Wellington was significantly lower than the other places, and it was discovered that high wind speed reduces the frequency of condensation on the surface of the collector.

The simulation was also run by using the data in Christchurch, the total number of simulated condensation hours in Christchurch for 2010 was 4130 hours which was considerably higher than Auckland. In Figure 29, it can be seen that the frequency of simulated condensation hours in winter is higher than the other cities. In Christchurch in winter, relative humidity is considerably high and the ambient temperature can drop below 0 °C at night, so ground frost is common in winter. It can be seen that the ambient temperature can be one of the climatic factors which influence the frequency of condensation.

The last location was Dunedin, and the annual number of simulated condensation hours was 3479 hours which was slightly higher than Auckland. Dunedin is one of the cloudiest cities in New Zealand and, the average temperature in Dunedin is generally lower than in Auckland throughout the year, consequently, the frequencies of condensation was slightly higher than Auckland.

It was found that the frequency of condensation on the surface of the cover was considerably influenced by three climatic factors: which are ambient temperature, wind velocity and relative humidity. It was found that areas with a low mean wind velocity and high relative humidity, such as Hamilton, and with cold weather, such as Christchurch, had a high frequency of condensation.

4-3-2 Influence of cover emissivity on condensation frequency

Figure 30 shows that the simulated absorber and cover temerature on July 1st in Auckland when the emissivity of the glass cover was 0.1 and 0.9. From this figure, lower cover emissivity made the absorber temperature higher especially during the day time. On the othe hand, changing emissivity of the glass did not influence the cover temperature significantly.

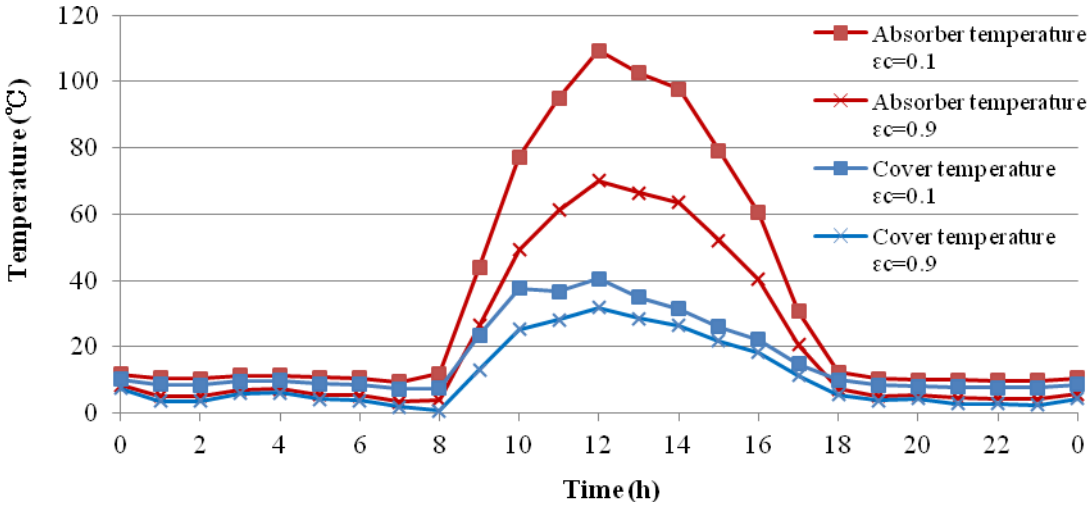

Figure 30: The simulated absorber and cover temperature on July 1st in Auckland when the cover emissivity is 0.1 and 0.9

Figure 31 shows the cover and absorber temperature at 12pm on July 1st in 2010. The emisivity of the cover was changed from 0.1 to 0.9. In Figure 31, the cover temperature was declining as linear function, in contrst, the absorber emissivity was decreasing as a quadratic function since radiant heat transfer is a function of T^4.

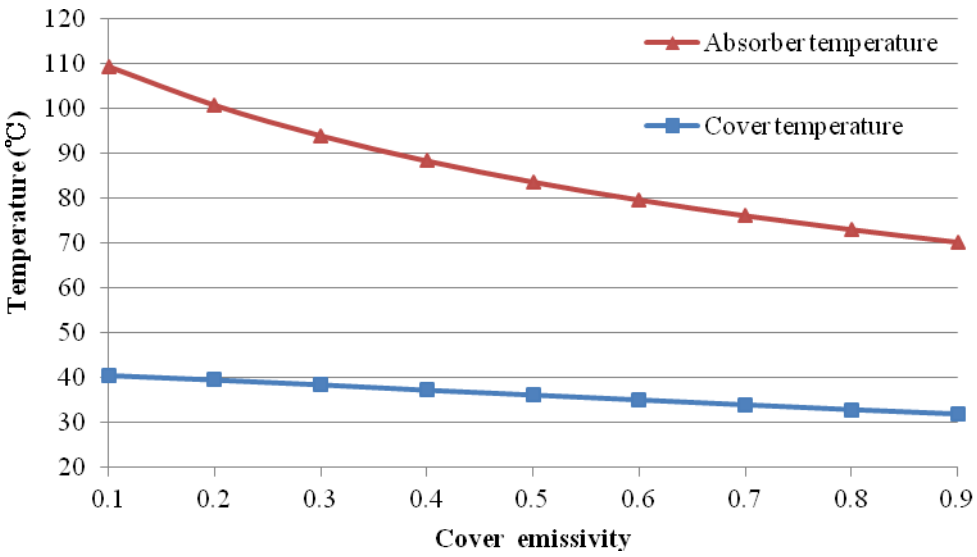

Figure 31: The relationship between the cover emissivity and the simulated absorber, cover temperatures

During the simulation, the emissivity of the cover was changed from 0.1 to 0.9 to determine the affect this on condesation frequency. Figure 32 shows the relationship of cover emissivity and the expected number of condensation hours in Auckland for 2010. The figure shows that cover emissivity significantly influences the frequency of condensation. As such, low emissivity glass is highly effective in preventing condensation. The simulation shows that using glass with an emissivity below 0.1 would prevent condensation on the surface of the glass of the collector throughout the year in Auckland.

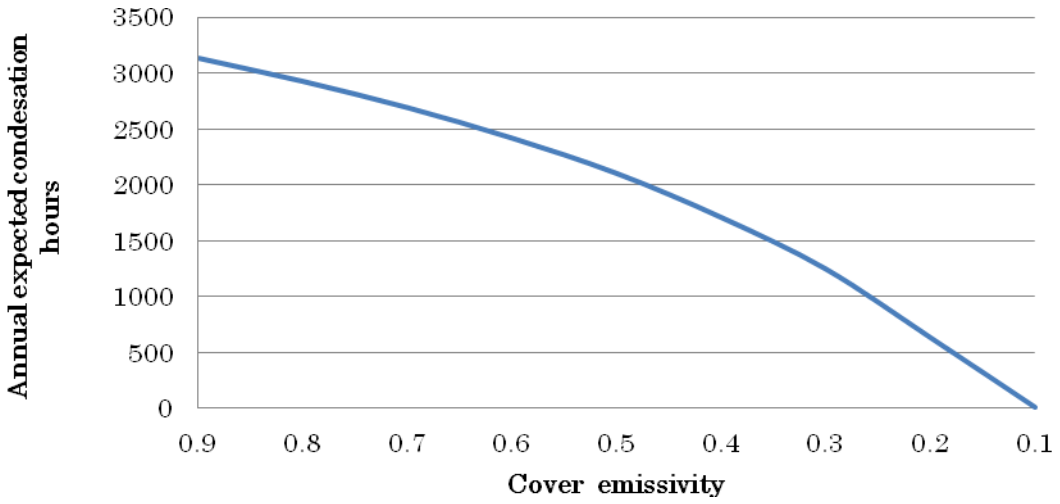

Figure 32: The relationship between cover emissivity and annual expected condensation hours

4-3-3 Influence of absorber emissivity on condensation frequency

Figure 33 shows that the simulated absorber and cover temerature on July 1st in Auckland when the emmisivity of the absorber was 0.1 and 0.9. From the figure, lower absorber emittance tends to show high absorber temperature, however it did not influence the cover temperature.

Figure 34 shows the relationship between absorber emissivity and the number of simulated condensation hours. From this figure, absorber emissivity does not influence the frequency of condensation on the surface of the collector.

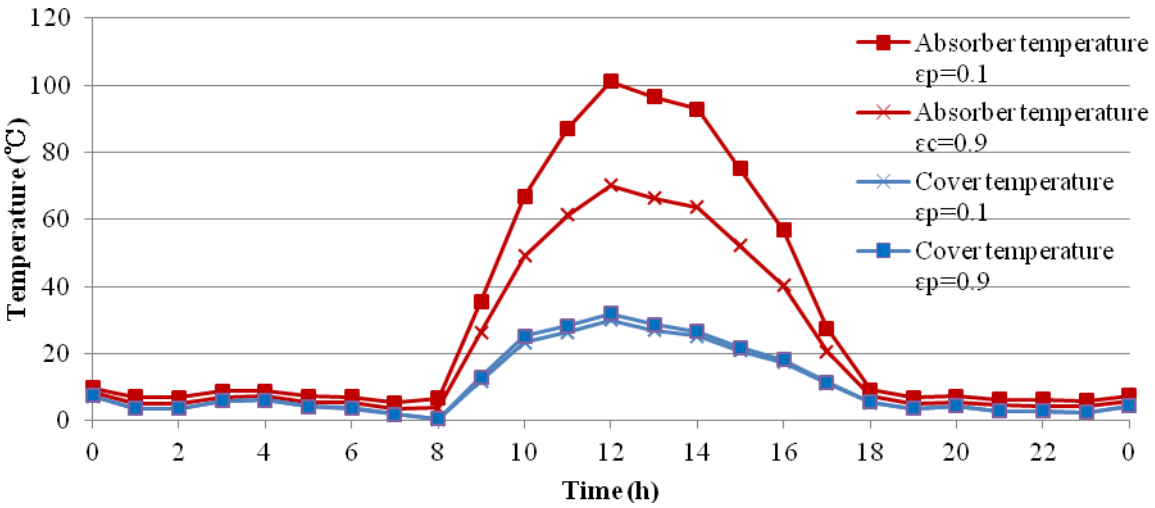

Figure 33: The simulated absorber, cover temperature when the absorber emissivity is 0.1 and 0.9

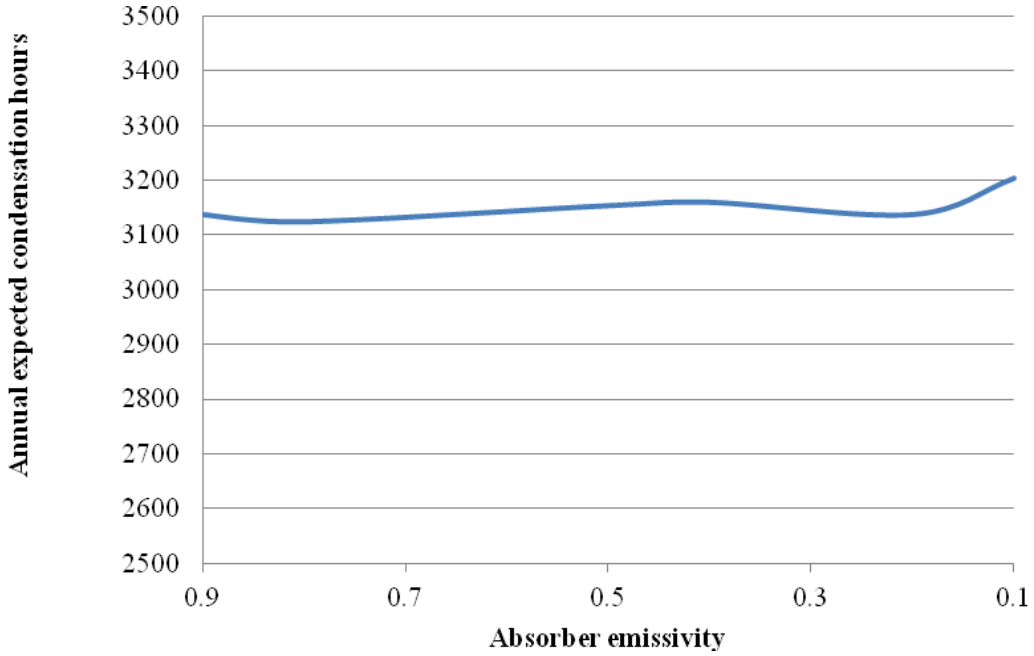

Figure 34: The relationship between the absorber emissivity and annual expected condensation hours

4-3-4 Influence of the slope of the collector on condensation frequency

The slope of the collector was also changed, the slope was set as 15°, 30°, 45° and 60°. Figure 35 shows the relationship between the number of expected condensation hours and slope of the collector. This indicates that incresing of the slope of the collector had an impact on condensation on the surface of the collector even though the difference was not as great as changing cover emissivity.

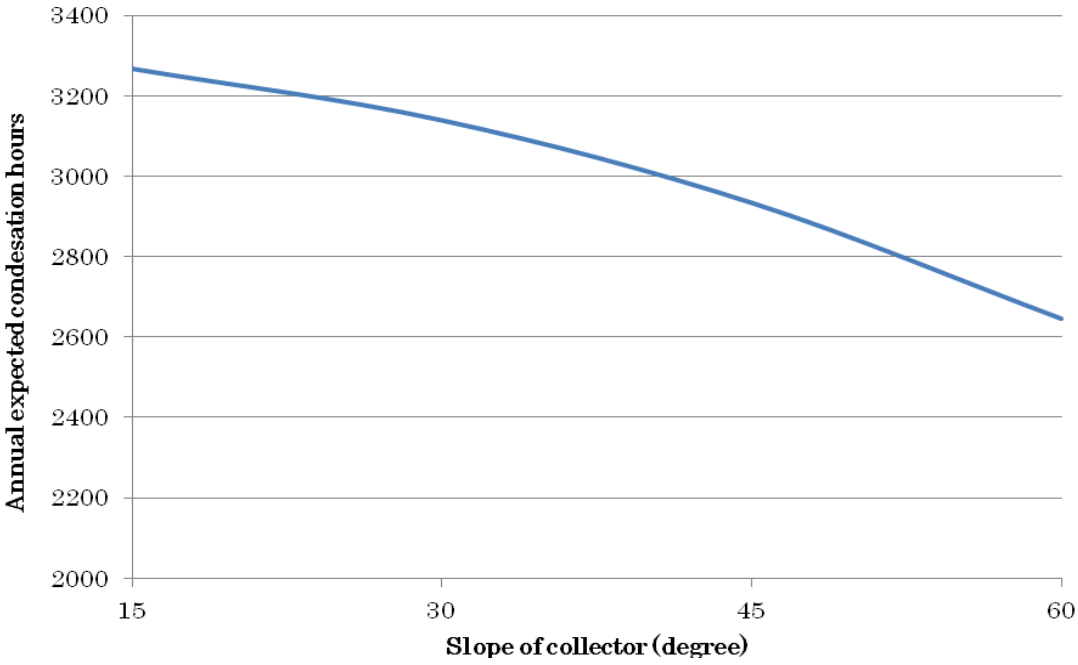

Figure 35: The relationship between the slope of the collecter and annual expected condensation hours

In the modeling, changing the slope of the collector influences two heat transfer parameters in equations (11) and (14). In Equation (11) , h_{cg}, represents the heat transfer coefficient for natural convection in the air gap, on the other hand, equation (14), h_{ro}, is the heat transfer coefficient for thermal radiation from the cover to ambient air. Figure 36 shows the relationship between the slope of the collector and h_{cg} and h_{ro} at night. At night, h_{cg} was not influenced by any collector slope. On the other hand, h_{ro} was decreased as increasing of slope of the collector. Figure 36 suggests that increasing of the slope of the collector decreses the thermal radiation from the cover to the ambient at night. Figure 37 shows the relationship between the slope of the collector and h_{cg} and h_{ro} during the day time. Both values were decreased as the slope of the collector increased.

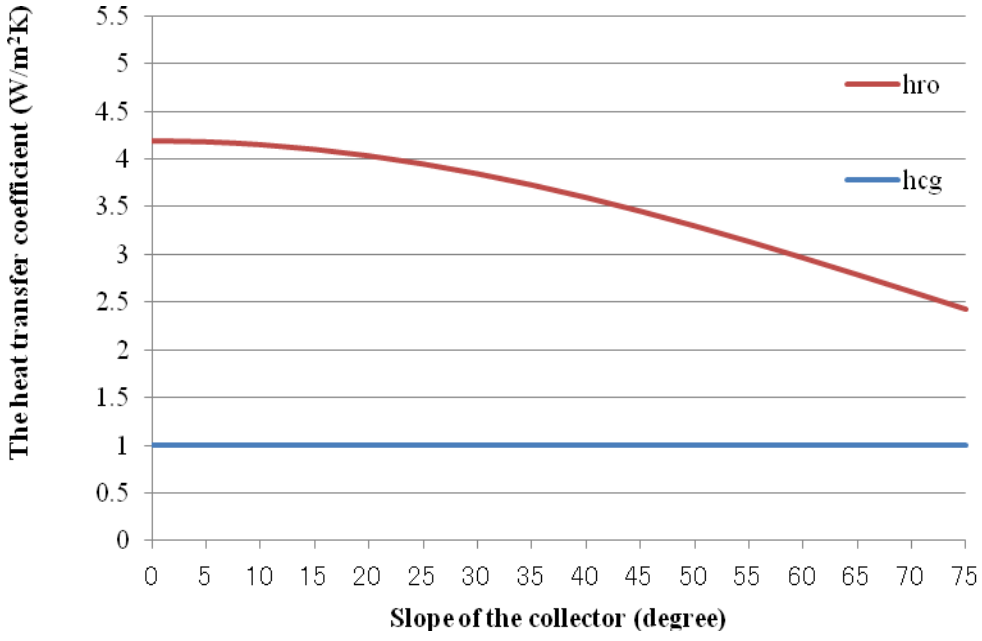

Figure 36: The relationship between the slope of the collector and h_{cg} and h_{rg} during the night

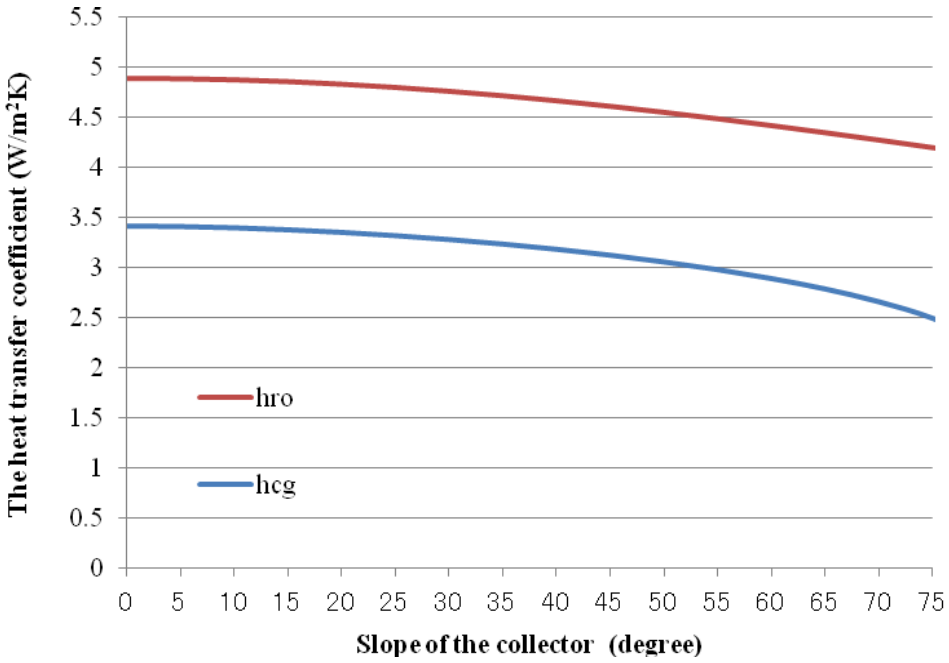

Figure 37: The relationship between the slope of the colector and h_{cg} and h_{rg} during the day time

4-3-5 Influence of the thickness of insulation on condensation frequency

The absorber and cover temperatures were compared when the thickness of insulation was 0.01 and 0.1 m as shown in Figure 38. From this Figure, during the day time, using thicker insulation were effective to keep the heat between the cover and absorber. The thickness of back insulation was changed from 0.01 to 0.1 m. Figure 39 shows the relationship between back insulation and the number of expected condesation hours for 2010 in Auckland. The thickness of back insulation did not significantly influence the frequency of condensation on the surface of the collector. The reason is that thickness of insulation influences the heat loss due to conduction in the back insulation more than the radiation from the cover. However, it should be noted that increasing the thickness of insulation will reduce heat loss

from the back of the absorber but lead to higher radiation heat from the front. The result of this will be a slight increase in condesation hours for e_i=0.1.

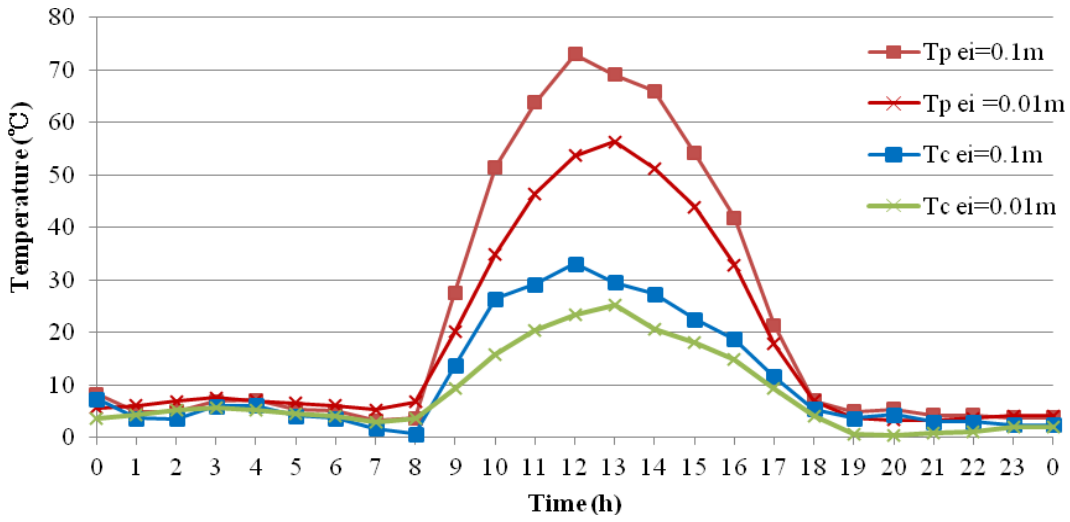

Figure 38: Absorber temperatures when the thickness of insulation is 0.1and 0.01

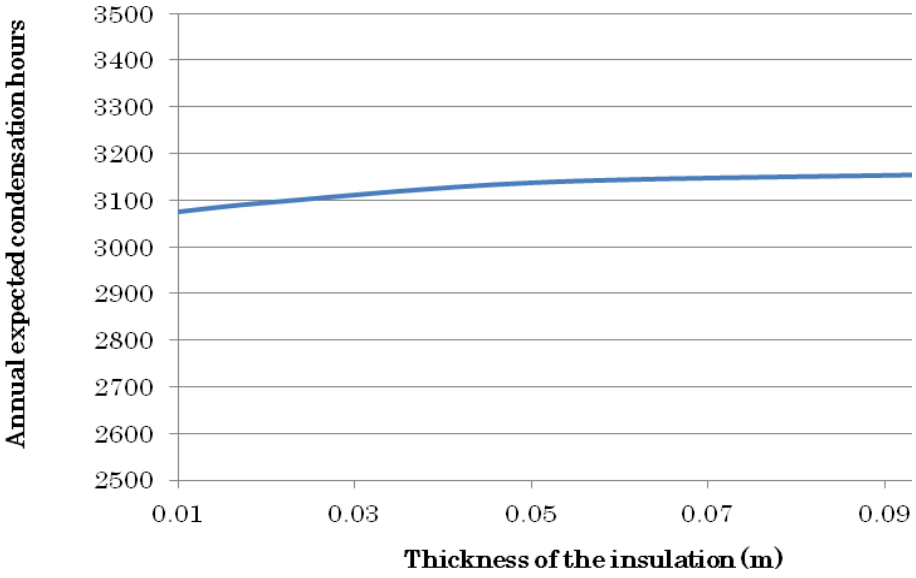

Figure 39: The relationship between the thickness of insulation and frequency of condensation.

4-3-6 Influence of ventilation of the air gap on condensation frequency

Ventilation of the air gap was expected to play an important role on the frequency condensation since it relates to the moisture movement in the air gap. Therefore, the relationship between ventiliation of the air gap and condesation on the outer cover was examined. Figure 40 (a) and (b) show the simulated absorber, cover temperatures when h_{vg} is 0.1, 10 and 40 W/m^{2}K. High h_{vg} means high ventilation of the air gap in the collector. Figure 40 (a) and (b) show the same trend that increasing ventilation eliminates the distinction between the temperature inside and outside the collector at night and during the day, it decreases the surface temperature of absorber and cover.

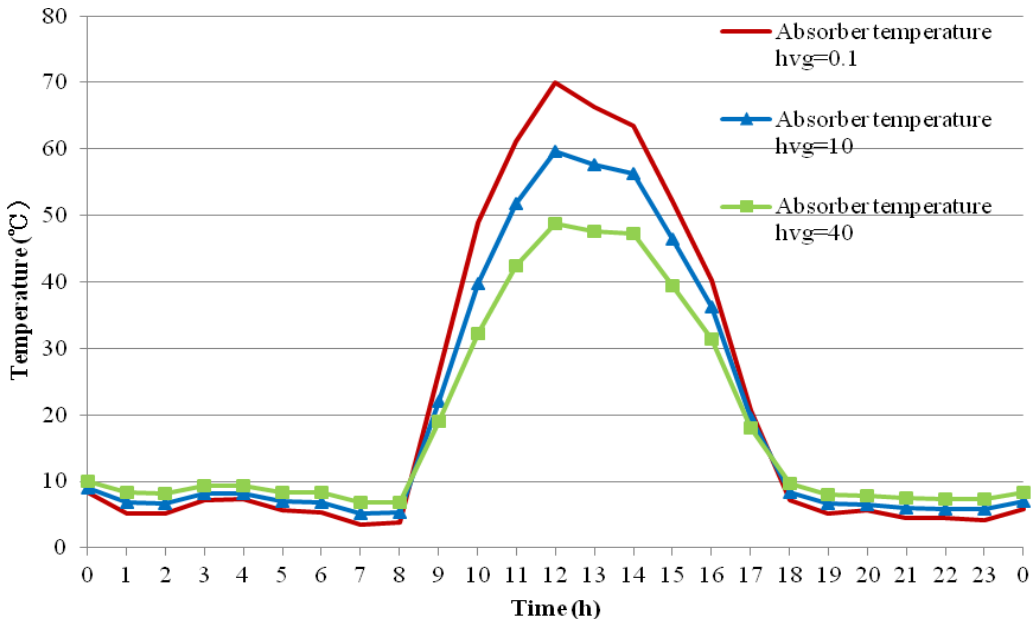

(a)

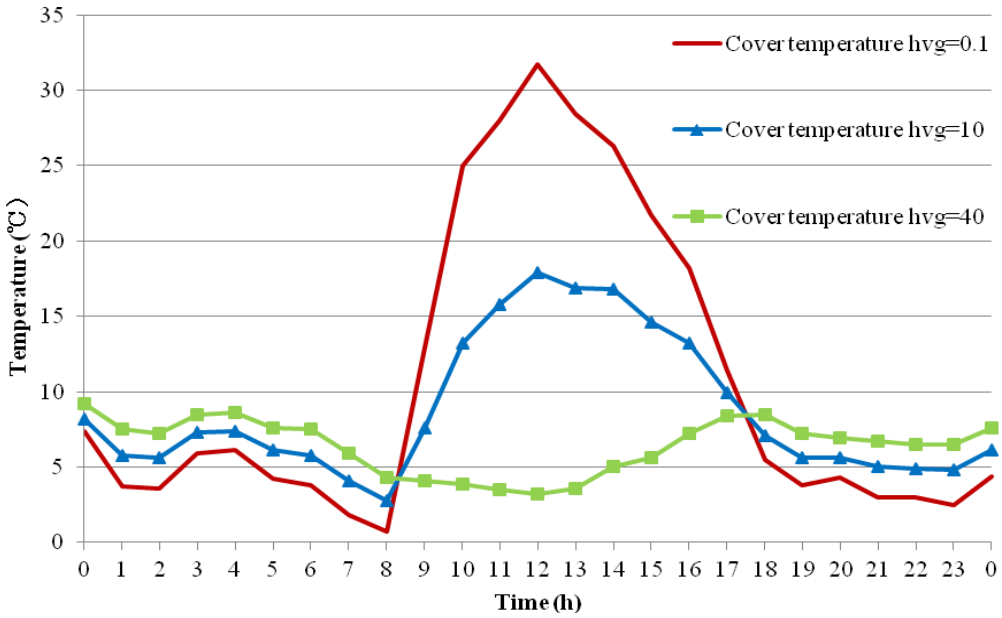

Figure 40: Temperatures when the ventilation rate is is 0.1, 10 and 40. (a) Absorber temperature, (b) Cover temperature

During the simulation, the convection heat transfer coefficient , as a proxy for the ventilation rate of the collector h_{vg} was changed from 0 to 40 W/m^{2}K. Figure 41 shows the relationship between ventilation rate and the number of expected condensation hours on the surface of the collector cover. It is shown that ventilation is effective in preventing condensation, however, high ventilation is not always effective.

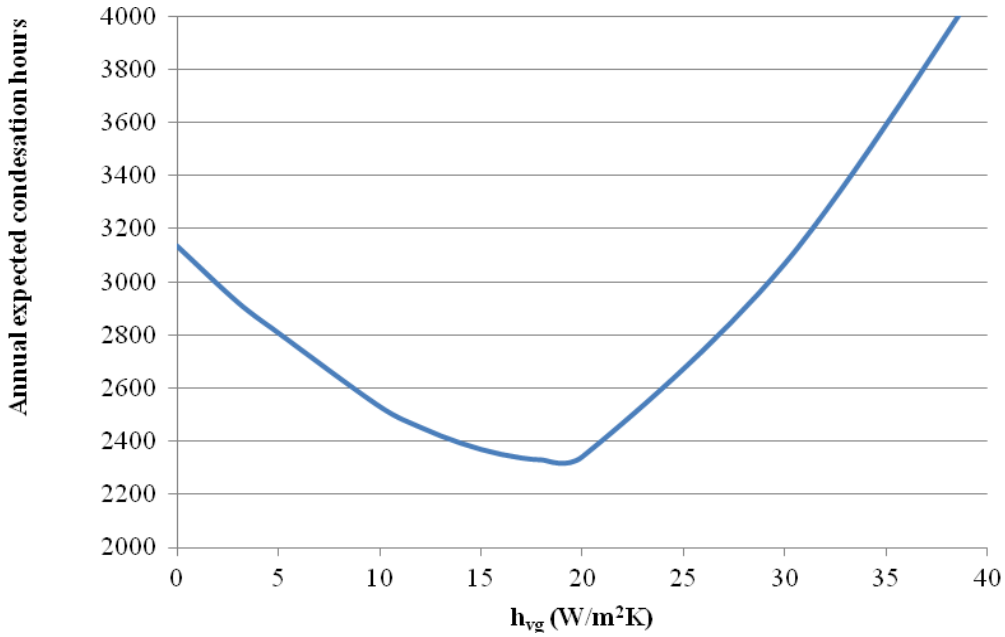

Figure 41: The relationship between ventilation rate and annual expected condesation

High ventilation sometimes increses moisture input and it is not able to maintain high temperatures for the absorber and cover surface. From Figure 40 and 41, ventilation is effective to prevent condensation when compared to stagnant conditions, however, high ventilation is not always effective to prevent condesation. This can be because of two important things to consider in controling the surface condensation (British Standard, 2005):

1, Gaining low vapor pressure by ventilation and reduced moisture input

2, Gaining high surface temperatures by providing insulation or heat input

The best solution is to keep the appropriate ventilation in the microclimate. And the downside to increasing uncontrolled ventilation is that it means higher heat loss during the day and so a lower collector efficiency.

4-3-7 Influence of the thickness of the air gap on condensation frequency

Figure 42 shows the absorber and the cover temperature when the thickness of the air gap was 0.01 and 0.025 m. The thinner air gap made absorber temperatures lower during the daytime. However, the thickness of the air gap did not influence the cover temperature considerably.

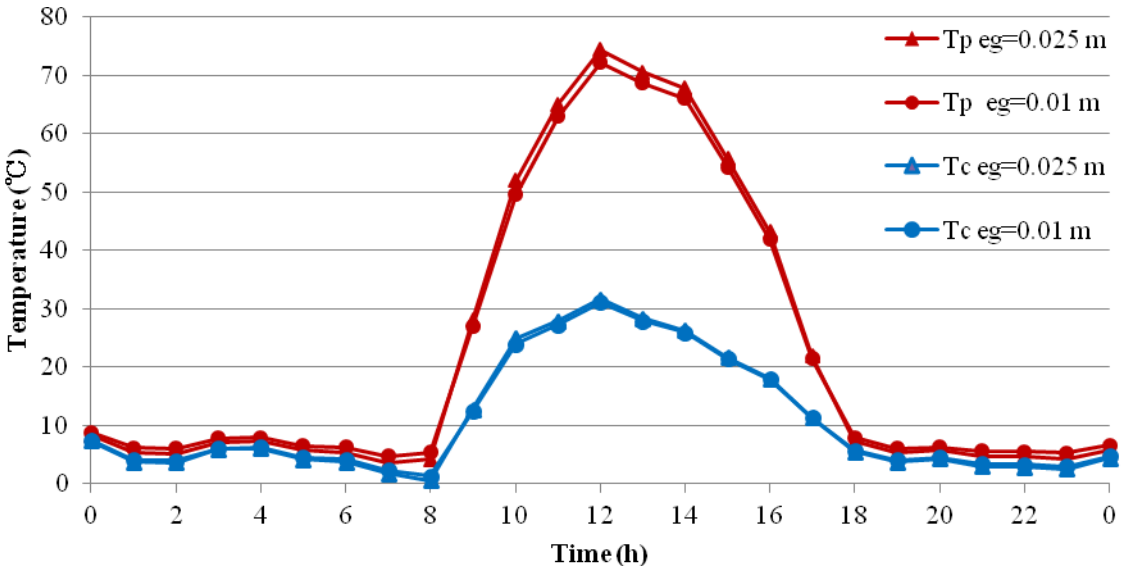

Figure 42: Absorber and cover temperatures when the thickness of the air gap is 0.01and 0.025

Figure 43 shows the relationship between the thickness of the air gap and the frequency of annual condensation. The simulated condensation hours are almost constant, so the air gap does not have an impact on the frequency of condensation on the surface of the collector.

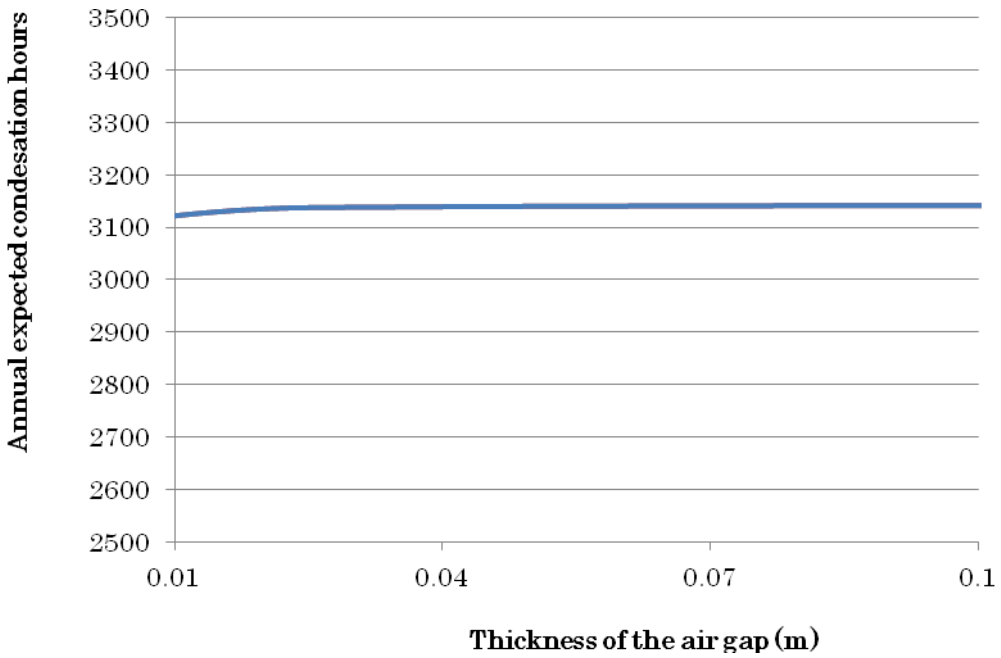

Figure 43: The relationship between thickness of the air gap and and annual expected condensation

4-4 Sensitivity of empirical correlation inputs

4-4-1 Dew point temperature prediction

When determining if condensation occurred in the collector system, the dew point temperature was used to compare to the cover temperature. During the simulation, the measured dew point temperature from NIWA'S annual weather data file (NIWA, 2012) was applied. However, there were also two equations (45) and (46) that could be used to calculate the dew point temperature. In a simple way, the dew point in Fahrenheit was described by equation (45) (Lawrence, 2005). On the other hand, Snyder et al (2005) published the method which described dew point temperatures by using the dry air temperature and relative humidity (Equation (46)). Those two equations were applied and compared with the measured values from NIWA'S annual weather data file (NIWA, 2012).

$$T_{dewa} = T - \frac{100 - RH}{5} \tag{45}$$

$$T_{dewa} = \frac{237.7\left(\frac{\ln(RH/100)}{17.27} + \frac{T}{237.3+T}\right)}{1-\left(\frac{\ln(RH/100)}{17.27} + \frac{T}{237.3+T}\right)} \tag{46}$$

Figure 44 shows a comparison of the measured dew point temperatures for 2010 in Auckland and the calculated dew point temperature from equations (45) and (46). Figure 44 shows that both equations predict higher temperatures than the measured dew point temperature from NIWA. However, equation (45) predicts closer dew point temperatures to the dew point temperatures from NIWA.

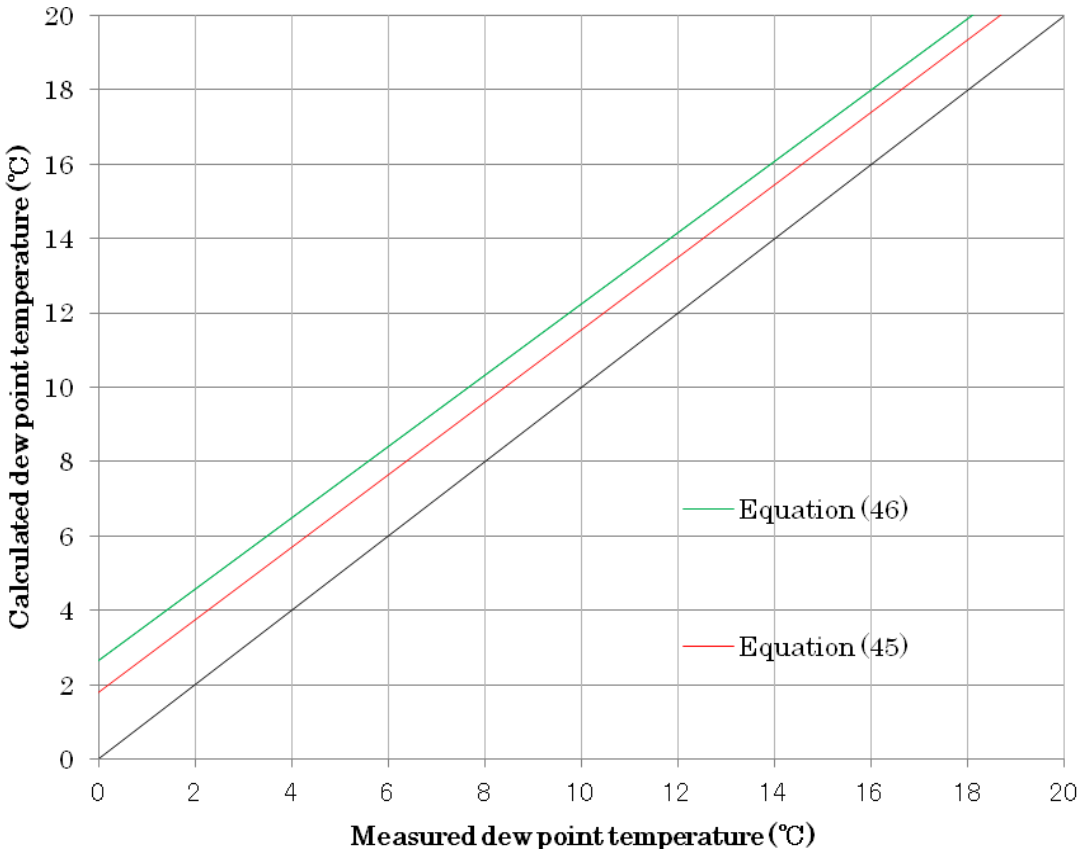

Figure 44: Relationship between measured and calculated dew point temperatures (Auckland)

There are several possible reasons why the dew point temperature from NIWA and calculated temperatures indicate different temperatures and equation (45) indicated closer dew point temperatures. It could be that the difference between the measured and calculated temperatures came from the error of the humidity sensor, since humidity sensors normally have an error range around 5%. In addition, the wind speed could influence the humidity sensor. (Harrison and Wood, 2011).

Figure 45 shows the dew point temperatures and wind velocity on a typical winter day in Auckland. In this figure, the both calculated dew point temperatures behaved as the same as the dew point temperature from NIWA except from 10am to 6pm. During 10am to 6pm, there is average 2 or 3℃ temperature difference, at the same time, the wind velocity increased to 5 m/s. From this figure, it can be seen that the wind could have influenced the measured dew point temperature.

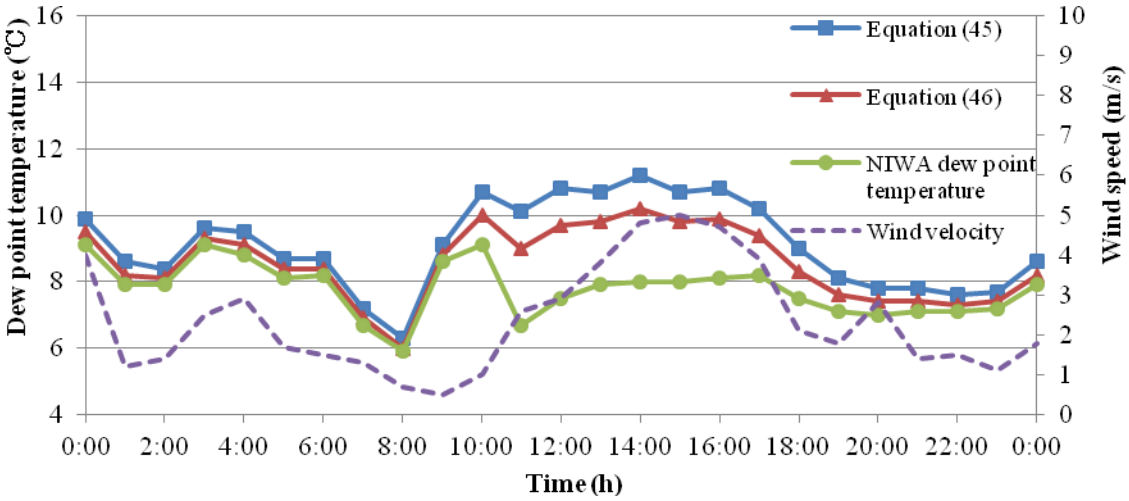

Figure 45: Dew point temperatures on a winter day in Auckland

Figure 46 shows the relationship between wind velocity and the temperature difference between the dew point temperature from NIWA and the calculated dew point temperatures. From this figure, as the wind velocity is faster, the error was increasing, and the wind velocity under 3 m/s the error was relatively small.

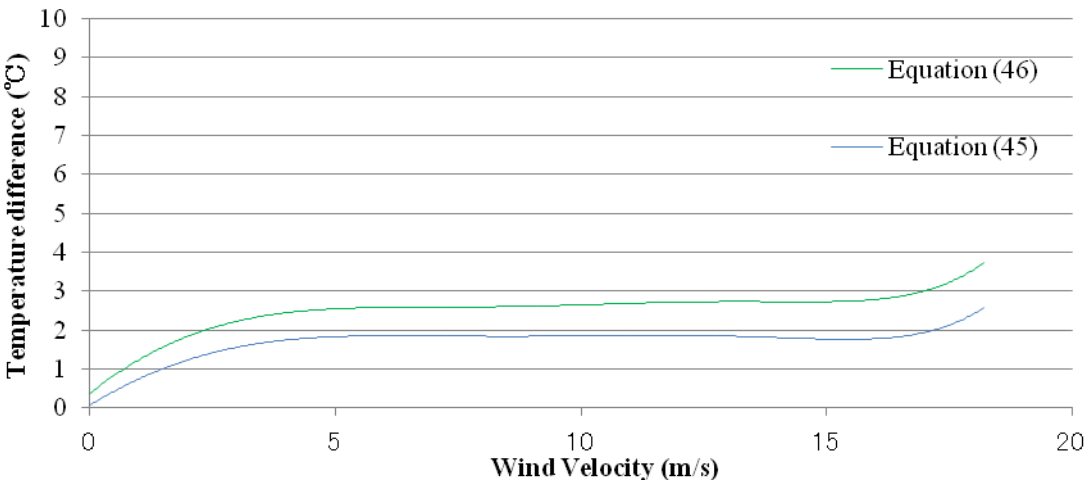

Figure 46: The relationship between wind velocity and the difference temperature from NIWA dew point and calculated dew point.

To examine the dew point calculation, the weather data from Hamilton and Wellington was used. The annual average wind velocity for 2010 in Hamilton was 2.8 m/s, in contrast, the average wind speed in Wellington was 8 m/s (NIWA, 2010). Figure 47 and 48 respectively show the relationship between dew point temperatures from NIWA and calculated dew point temperatures in Hamilton and Wellington. From these figures, Wellington which tends to have higher wind speeds showed a significant difference between the dew point temperatures from NIWA and calculated dew point temperatures. Winds influence dew point temperatures and it is important to consider wind velocity, especially if the location has wind speeds over 3 m/s.

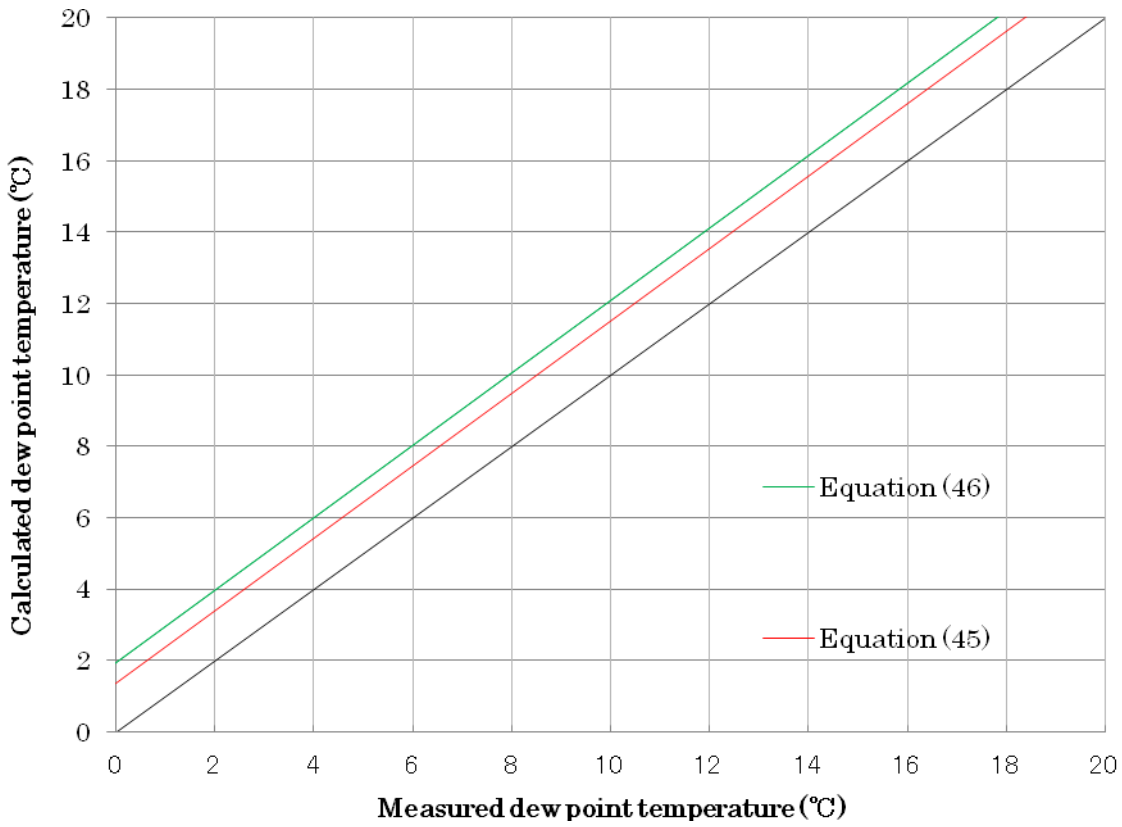

Figure 47: Relationship between measured and calculated dew point temperatures

(Hamilton)

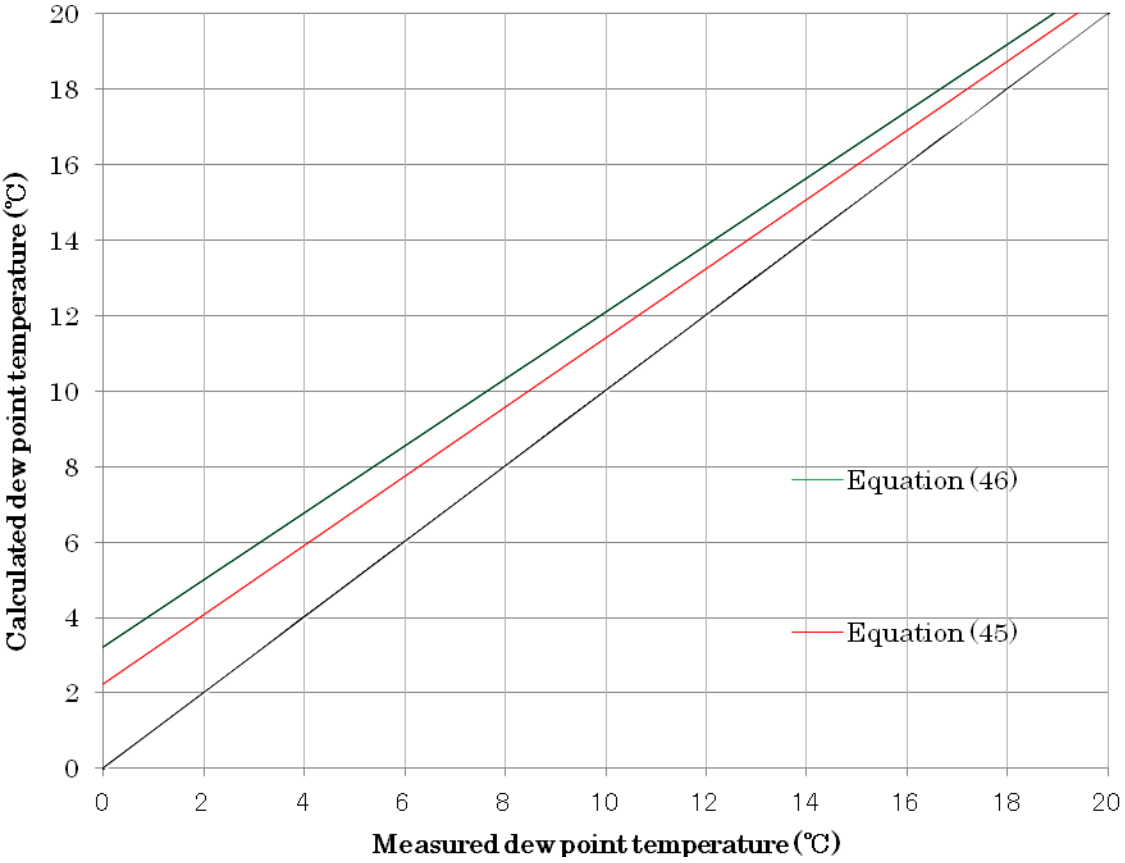

Figure 48: Relationship between measured and calculated dew point temperatures (Wellington)

Figure 49 shows the relationship between expected condensation hours in Auckland 2010 using the measured dew point temperature and the simulated dew point temperatures which were obtained from equation (45), (46). From Figure 49, the measured and simulated dew point temperatures showed the same trend, however, both simulated data sets showed a higer number of condesation hours. Consequently, both equations can be applied to understand the trend. However, there are some minor difference between dew point and simulated dew point temperatures and its influence on the frequency of condensation on the surface of the collector.

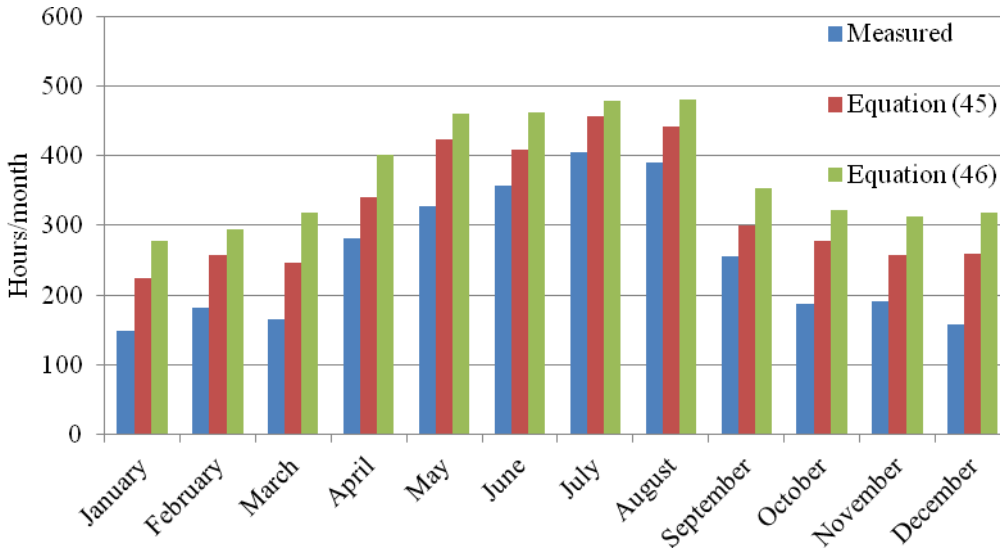

Figure 49: Expected monthly condensation hours for 2010 in Auckland

4-4-2 Influence of the sky temperature equations on predicted condensation frequency

The surface of a collector exchanges radiation to the cold sky. Kohl et al (2004) suggested the equation (5), on the other hand, Duffie and Beckman (2006) also published an equation to calculate the sky temperature. The equation (5) determines the sky temperature in a simple way. In contrast, equation (6) is strengthened through the inclusion of a time and dew point temperature factor. Both sky temperatures were calculated from equations (5) and (6), and were compared to the weather data from NIWA.

$$T_s = 0.0552 \cdot T_a^{1.5} \tag{5}$$

$$T_s = T\left[0.711 + 0.0056T_{dp} + 0.000073T_{dp}^2 + 0.13\cos(15t)\right]^{\frac{1}{4}} \tag{6}$$

Equation (5) and (6) are effective only for clear sky conditions, however, in the absence of an appropriate cloudy sky temperature model, the equations were employed to calculate the sky temperature. Figure 50 shows the simulated sky temperatures which were calculated from equation (5) and (6). The weather data was collected from a winter day in Auckland in 2010 (NIWA, 2010). Both equations show the same trend, however, it seems at night the difference between the sky temperatures from equation (5) and (6) are greater than during the day. The impact of this would be an overprediction if the frequency of condensation occurring.

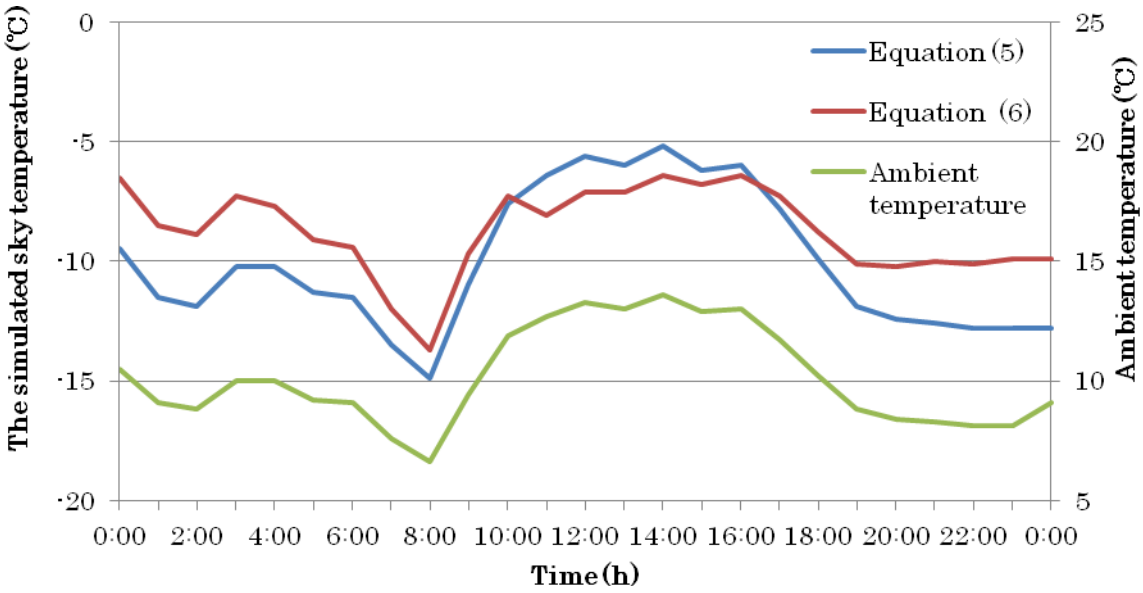

Figure 50: The simulated sky temperature and ambient temperature on a winter day in Auckland.

Figure 51 shows the simulated cover temperature when equations (5) and (6) were used for sky temperature. From the Figure, although both simulated cover temperatures showed almost the same temperature during the day, at night the cover temperature from equation (5) was slightly higher.

The expected condensation hours in Auckland in 2010 when the equations (5) and (6) were used for sky temperature was 3059 and 3429 hours respectively. Equation (5) tends to show lower sky temperatures compared to equation (6) and as a result, equation (5) showed high frequency of simulated condensation hours even though the weather data was exactly the same. From Figures 50 to 52, the sky temperature influences the cover temperature and, the sky temperature has an impact on the frequency of condesation. And it should be noted that both equations are effective for clear sky conditions, consequently, the frequency of condensation will be overpredicted.

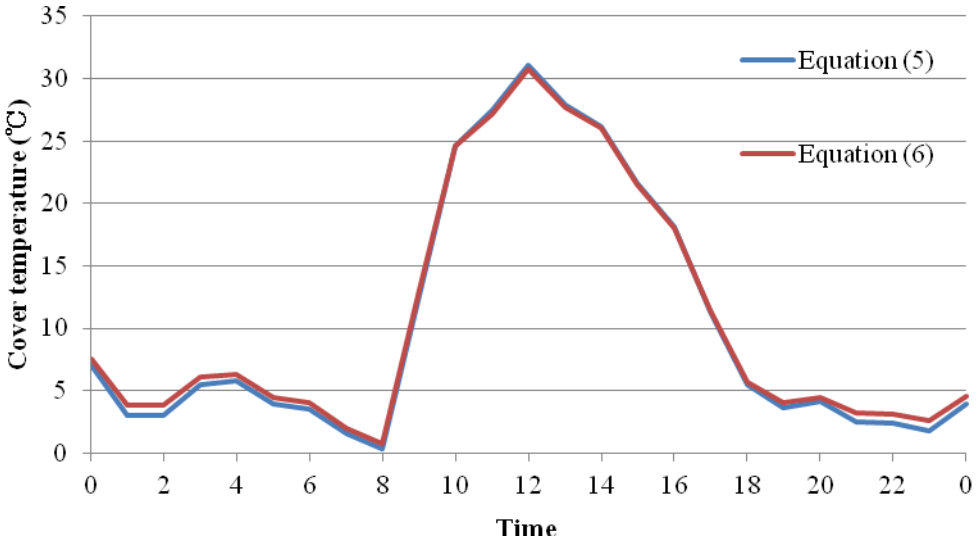

Figure 51 : Simulated cover temperature which equation (5) and (6) were used for sky temperature

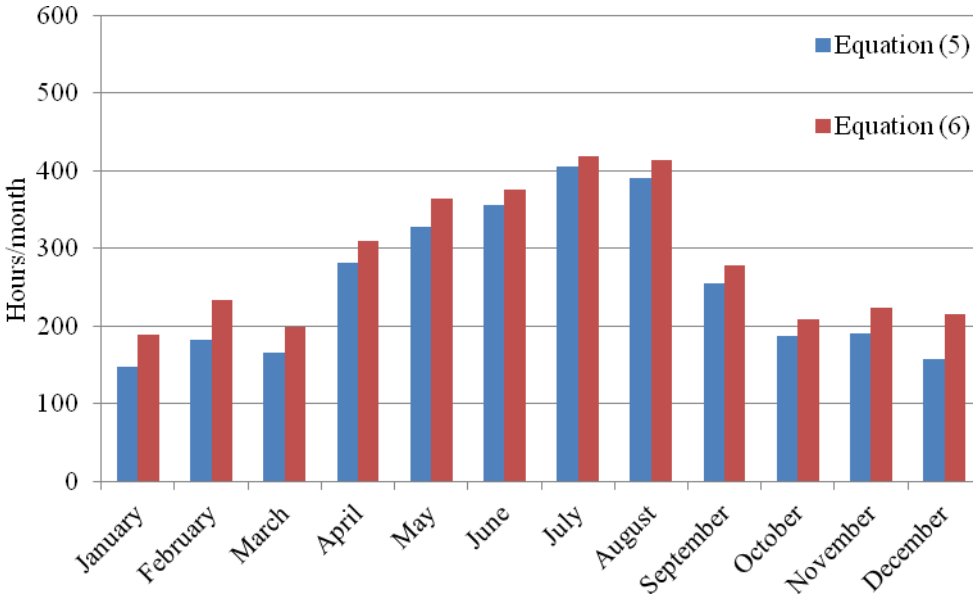

Figure 52: Expected monthly condensation on the solar collector in Auckland when equation (5) and (6) were applied for sky temperature

4-4-3 Effect of heat convection transfer correlation and its affect on condensation frequency

In this study, condensation on the surface of the cover was considered, so estimating the convective heat transfer coefficient due to wind is important. During the simulation, the wind speed was artificially changed at a constant speed from 1 m/s to 5 m/s. As expected, the frequency of condensation decreased as increasing the wind velocity as shown Figure 53.

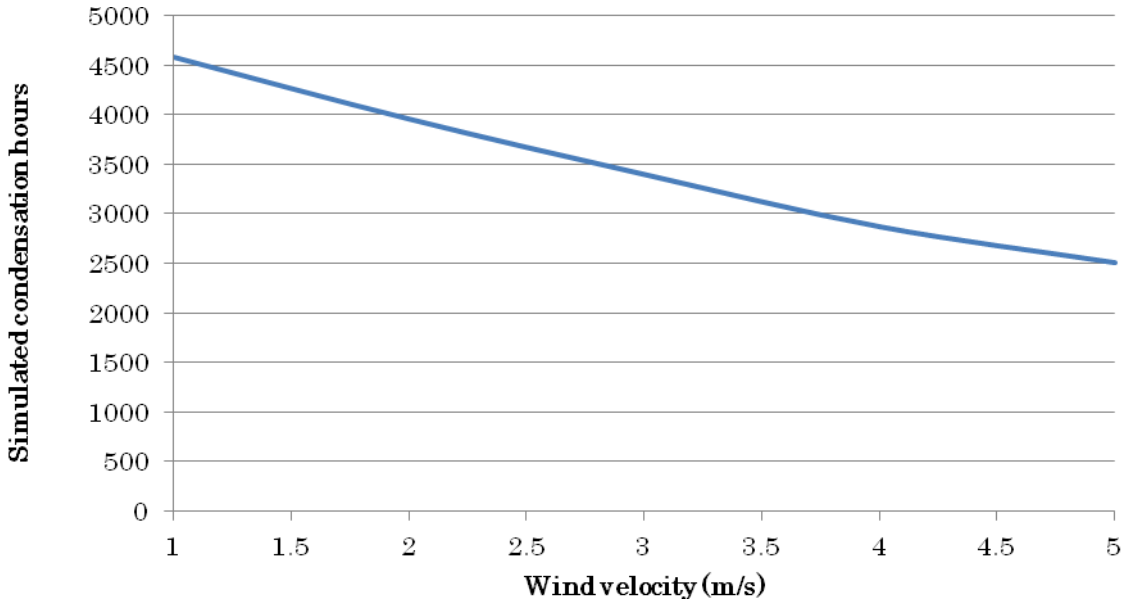

Figure 53: The relationship simulated condensation hours and wind velocity

In the model, the heat transfer by convection from the cover to the ambient air was calculated from the equation (15). This equation contains natural convection and forced convection from the cover to the ambient air. However, Sharma et al (1997) published two different equations (equation (1) and (2)), which considered only forced convection. Figure 54 shows the cover temperature which equation (15), (1) and (2) were used to calculate the heat convection from the cover to the ambient air.

$$h_w = 5.7 + 3.8V_w \quad (1)$$

$$h_w = 10.03 + 4.687V_w \quad (2)$$

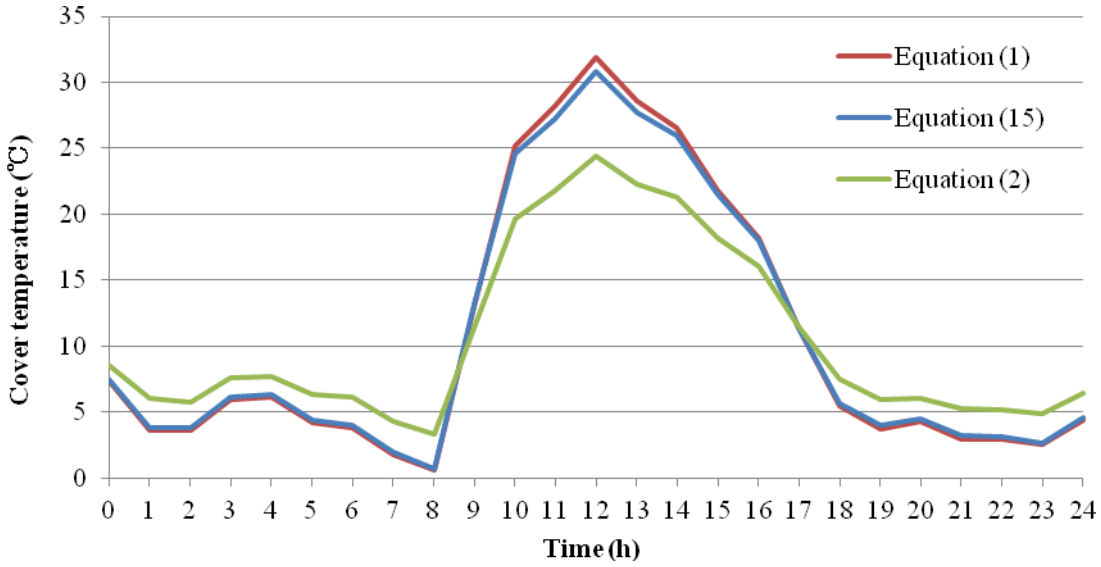

Figure 54: Cover temperatures when equation (15), (1) and (2) were used to calculate the heat convection from the cover to the ambient air

During the simulation, the three equations were used and compared to simulate the frequency of the condensation. Figure 55 shows that expected condensation hours which calculated from equations (15), (1) and (2). The expected condensation hours were respectively 3049, 3138 and 2054 hours. Equation (15) and (1) showed similar expected condensation hours, however, there was almost 1000 hours difference between equation (15) and (2). From Figure 53 to 55, wind velocity plays a significant role on temperature and the condensation frequency on the surface of the collector and, equation (15) could be substituted for equation (1).

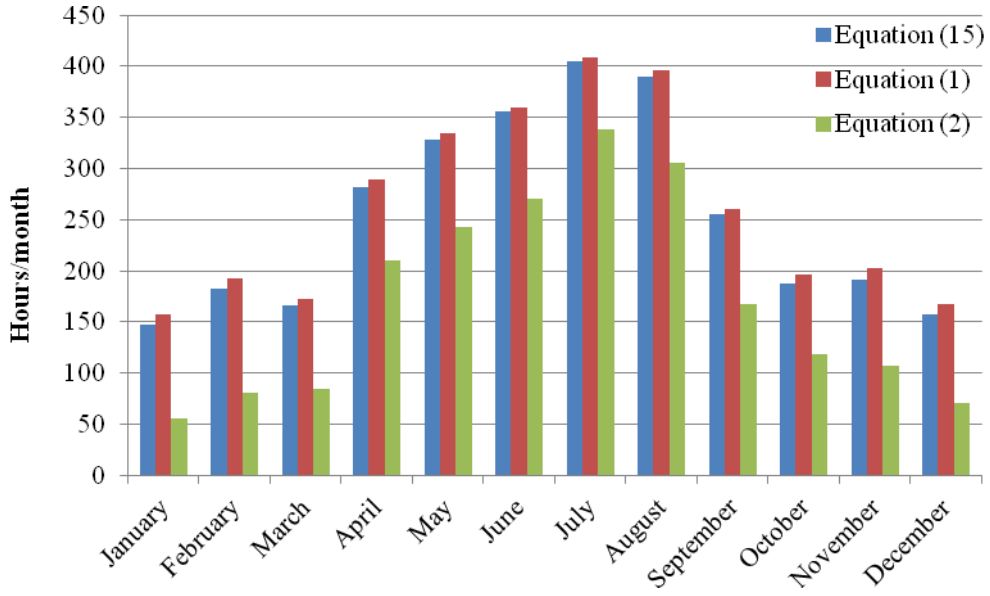

Figure 55: Expected monthly condensation on the solar collector in Auckland when the equation (15),(1) and (2) were applied

Chapter 5: Discussion

Gaining an understanding of condensation in solar collectors is important in terms of their durability and performance. Wetness on the absorber of the solar collector can damage the surface and cause corrosion on the absorber plate. In addition, the build-up of condensation on the glazing means energy must be wasted to evaporate the moisture during the following day. The objective of this research was to understand the microclimate inside the collector to prevent the occurrence of condensation on a surface of the collector. The model helped to predict the important factors: absorber, cover temperature and also relative humidity inside the collector. This section will highlight and discuss the main four findings and explore the improvements of the model.

5-1 A microclimate exists inside the collector

In the experiment, relative humidity inside and outside the collector were measured. The primary finding was that a microclimate exists inside the solar collector since relative humidity inside the collector behaved differently to the relative humidity outside as shown in Figure 22. Relative humidity inside dropped rapidly in the morning and increased as sun went down. The reason is that the amount of the saturated vapor depends on the air temperature, and in the day time the temperature inside the collector reaches high while after sunset, the temperature inside the collector decreases. As a result, relative humidity decreases in the morning and rises at night.

5-2 Model validation

The model helped to predict the important factors: absorber, cover temperature and also relative humidity inside the collector. In Figure 23, the simulated absorber temperature fluctuated due to the variation in the incident radiation, however, the simulation was able to predict the absorber temperature relatively well. In Figure 24 and 25, the simulated cover temperature and relative humidity inside showed almost the same temperature as the measured temperature and relative humidity. To examine the model, a verification test was also conducted. In Figure 26, some moisture was found on the collector at 8am and, the model predicted that condensation might have occurred until 7:30 am as shown in Figure 27. The location was not exactly the same as the test site because the weather information from the NIWA Cliflo database was collected and applied to the simulation. Therefore, the condensation persists slightly longer than the model would predicted.

5-3 Sensitivity analysis

5-3-1 Climate factors

The weather data from five different places in New Zealand, namely Auckland, Hamilton, Wellington, Christchurch and Dunedin were simulated and compared with each other to understand the main climate factors which determine frequency of condensation and, each simulation data featured its own special weather characteristics. In Figure 29, the cities that had the most frequent condensation were Hamilton and Christchurch and the city with the lowest incidence of condensation was Wellington.

It was found that the frequency of condensation on the surface of the cover was considerably influenced by three climatic factors which were ambient temperature, wind velocity and relative humidity. In an area with a low mean wind velocity and high relative humidity, such as Hamilton a high frequency of condensation results; on the other hand, Wellington which has a high wind speed had low frequency of condensation.

5-3-2 Parameters which can alter the frequency of condensation

During the simulation, many parameters were changed and simulated, however, only three factors: the cover emissivity in Figure 32, the slop of the collector in Figure 35 and ventilation in Figure 41 had an impact in reducing the frequency of condensation.
The most effective way to reduce the condensation was by using low emissivity glass because it prevents thermal radiation at night. In addition, increasing the slope of the collector slightly decreased the frequency of condensation on the surface of the collector. The reason is that increasing of the slope of the collector decreases the thermal radiation from the cover to the ambient at night.

Holck et al. 2003 also stated that the occurrence of condensation increases with higher rate of ventilation. The possible reasons are high ventilation sometimes increases moisture input and, it is not able to maintain high temperatures for absorber and cover surface. However, increasing the ventilation rate is effective in preventing condensation when compared to stagnant conditions as shown Figure 41. Consequently, the best solution for this is to keep the appropriate ventilation in the microclimate.

5-4 Sensitivity of empirical correlation input

5-4-1 Dew point temperature

Condensation on the glazing occurs when the cover temperature falls below than the dew point temperature, so the dew point temperature is one of the important factors to consider in the occurrence of condensation. There were two equations to calculate the dew point temperature, equations (45) and (46), which were compared with actual measured data from NIWA. Both simulated dew point temperatures showed higher temperatures than measured temperatures from NIWA, but the dew point temperature which was obtained from equation (45) was closer to the measured dew point temperature from NIWA in Figure 48. The frequency of expected condensation hours which was obtained from the measured dew point temperature and two simulated dew point temperatures showed a minor difference in Figure 49, so the both simulated temperatures could be used instead of the measured temperature.

5-4-2 Sky temperature

At night, the glazing of the collector exchanges radiation with the night sky, so the sky temperature is a key to predicting condensation on the collector. However, it is difficult to measure the sky temperature. In this study, equations (5) and (6) were used and, the results were compared in Figure 51.

Those equations were simulated and a comparison made of how they influence the frequency of condensation in Figure 52. The difference of frequency was 500 hours for the whole year in Auckland and both equations are effective for clear sky conditions rather than cloudy or partly cloudy skies, consequently the frequency of condensation might have been overpredicted. Choosing the equation for the sky temperature is also a key to predicting the collector performance.

5-4-3 Heat convection transfer from the cover to the ambient air

This study highlighted condensation on the surface of the cover, so considering the convective heat transfer due to wind is important. Three equations (15), (1) and (2) were used to calculate the convective heat transfer from the cover to the ambient. Equation (15) contains natural and forced convection, on the other hand, Equation (1) and (2) considered only forced convection. The three equations were compared in terms of cover temperature in Figure 54, the frequency of condensation was also compared in Figure 55. Equation (15) and (1) showed almost the same cover temperatures and similar expected condensation hours, however, there was a significant temperature difference and almost 1000 hours difference in predicted condensation hours for equations (15) and (2). It was discovered that wind speed played an important role on the condensation frequency on the surface of the collector and equation (15) could be substituted for equation (1).

5-5 Three improvements of the model

The model predicted the main trend, however, the model still has minor differences from actual data. The first reason is that in the model there is a lack of consideration of strong winds. Strong winds make the error significantly wider since convection on the surface of the collector is mainly dominated by the wind velocity rather than natural convection. It is essential to discover a more accurate equation which expresses the heat conduction on the surface due to wind. In addition, during the calculation, the vapor pressure inside and outside was assumed to be the same. Finally, it was not possible to determine the clear sky temperature and cloudy sky temperature due to a lack of correlations to describe the sky temperature under cloudy conditions. To make a more accurate model, it is important to consider the difference vapor pressure inside and outside the collector and to develop an appropriate cloudy sky temperature correlation.

To sum up, the model indicates that climatic factors which are ambient temperature, wind speed and relative humidity play an important role in determining the frequency of condensation. However, the frequency of condensation can be modified by using low emissivity coating, increasing the slope of the collector and altering the ventilation rate. In the model there is still room for improvements, such as considering the effect of wind and the assumptions in the calculation; however the model is a significant starting point for predicting and optimizing the microclimate inside the collector.

6: Conclusions and future work

Solar thermal collectors are becoming commonly used around the world as a simple and effective method of heating water. Avoiding condensation in solar collectors at night is a crucial problem in terms of their durability and performance.

This study has shown that there are some key points to understanding condensation problems. A microclimate exsits inside the collector, and several climate factors influence the frequency of condensation, such as ambient temperature, relative humidity and wind velocity. However, these factors can be modified by altering the ventilation inside the collector, the slope of the collector and by using low emissivity coating. In addition to this, the equations of dew point temperature, sky temperature and convective coefficient on the surface due to the wind still need to be considered carefully since these parameters considerably influence the predicted frequency of condensation.

This model is helpful in the prediction of absorber and cover temperatures and it also gives an insight into the relative humidity inside of the collector. However, the numerical model focused on condensation on the outer surface of the cover, it is also important to consider the inner cover of condensation including moisture in insulation. Secondly, the inclination of the collector influences the frequency of condensation but it is typically chosen to optimize the year – round capture of incident solar radiation. To maximize the overall performance of the solar collector, it is important to consider all aspects which are influenced by the inclination of the collector. It was also concluded that appropriate ventilation was effective to prevent condensation, so next step is how to define ‘appropriate ventilation’. These could form the basis for future work in the area.

References

Argiriou, A., Santamouris, M and Assimakopoulos (1994) Assessment of the radiative cooling potential of a collector using hourly weather data. *Energy, 19*, (8), pp 879–888

ASHRAE (2009) *2009 ASHRAE Handbook of Fundamentals*, American society of heating, refrigerating and air-conditioning engineering, Inc. Atlanta, GA 30329.

British Standard (2005) *Code of practice for control of condensation in buildings*., London

Dickens, H (1963) The condensation problem – here are the causes and cures. *Canadian builder* XⅢ, 7, p34

Duffie, J and Beckman, W (2006) *Solar engineering of thermal processes, 3rd edition.* New Jersey: John Wiley&Sons,Inc

Duffie, J and Beckman, W (1991) *Solar engineering of thermal processes, 2nd edition.* New Jersey: John Wiley&Sons,Inc

Government of Bermuda/Department of energy (2012) Renewable energy guide: solar hot water systems Retrieved from Department of Energy website www.energy.gov.bm [cited 1/06/2012]

Harrison, R and Wood,C (2012) "Ventilation effects on humidity measurements in

thermometer screens", *Quarterly Journal of the Royal Meteorological Society 138*, pp 1114-1120,

Holck, O., Svend, S., Brunold, S., Frei, U., Kohl, M., Heck, M and Oversloot, H (2003) Solar collector design with respect to misture problems, *Solar Energy 75*, pp269-276,

Jain, P (2011) *Wind energy engineering*. The United States of America, The McGraw-Hill Companies, Inc.

Kohl, M.,Carlsson,B.,Jorgensen, G. and Czanderna, A., (2004) *Performance and durability assessment: Optical materials for solar thermal systems*. Oxford, Elsevier Ltd

Kohl, M.,Kubler, V and Heck, M., (2007), Optimisation of the micro-climate in solar collectors, *Solar Energy Materials & Solar Cells 91*, pp 721-726

Kreith, F. and Kreider, J., (1973), "Numerical prediction of the performance of high altitude balloons" Retrieved from http://nldr.library.ucar.edu/repository/assets/technotes/asset-000-000-000-055.pdf [cited 1/06/2012]

Moller, G. (n.d.). Solar water heating – Corrosion and performance issues in New Zealand. June 1, 2012, Retrieved from http://rustypanelsblog.blogspot.co.nz/ [cited 1/05/2012]

Parker, D.,(2005), “Theoretical evaluation of the night cool nocturnal radiation cooling concept” Retrieved from http://www.fsec.ucf.edu/en/publications/pdf/FSEC-CR-1502-05.pdf [cited 1/06/2012]

Renr, H., (2004), Construction of a generalized psychrometric chart for different pressures, *The International Journal of Mechanical Engineering Education*, *32*, pp 212-222.

Sharma, S.,Kandpal, T and Mullick, S (1997) Wind induced heat losses from outer cover of solar collectors *Renewable Energy*, *10*, pp. 613-616

The AUT weather data server http://weather.aut.ac.nz/weather/ServletTest.html [cited 1/3/2012]

The National Institute of Water and Atmospheric Research (2010) Cliflo database http://cliflo.niwa.co.nz/ [cited 1/12/2011]

The National Institute of Water and Atmospheric Research (2012) Cliflo database http://cliflo.niwa.co.nz/ [cited 2/03/2012]

Appendix